Characterization of Cholinergic mediated α7 and α4β2 Nicotinic Acetylcholine Receptor Responses in Layer1 Interneurons of the Medial Prefrontal Cortex

By

Mohammad Foad Abazari

A Thesis Submitted in Partial Fulfillment of the
Requirements for the Degree of

MASTER OF SCIENCE

in the Division of Medical Sciences (Neuroscience)

We acknowledge and respect the Lək̓ʷəŋən (Songhees and Xʷsepsəm/Esquimalt) Peoples on whose territory the university stands, and the Lək̓ʷəŋən and W̱SÁNEĆ Peoples whose historical relationships with the land continue to this day

Graduate committee

Characterization of Cholinergic mediated α7 and α4β2 Nicotinic Acetylcholine Receptor Responses in Layer1 Interneurons of the Medial Prefrontal Cortex

By
Mohammad Foad Abazari

Supervisory Committee:

Dr. Raad Nashmi, Department of Biology, University of Victoria (Supervisor)

Dr. Kerry R. Delaney, Department of Biology, University of Victoria (Outside Member)

Dr. Craig E. Brown, Division of Medical Sciences (Neuroscience), University of Victoria

Abstract

The medial prefrontal cortex (mPFC) is a brain region responsible for a variety of cognitive functions including attention and working memory. Cholinergic neurons, which release acetylcholine (ACh), are known to enhance attention and their pathophysiology is associated with disorders such as Alzheimer's disease and epilepsy. Nicotinic acetylcholine receptors (nAChRs) are activated by the cholinergic system and modulate neuronal excitability. Therefore, understanding nAChR mediated synaptic neurotransmission will allow us to better understand how the activity of neurons is precisely controlled.

Using whole cell recordings of layer 1 neurons of mouse mPFC and optogenetic stimulation of ACh release resulted in two nAChR mediated currents, one having a rapid rise and decay kinetics and sensitive to inhibition by the α7 nAChR antagonist MLA. The second nAChR current was long lasting and inhibited by the α4β2 nAChR antagonist DHβE. The α4β2 current was significantly inhibited by the calcium chelator EGTA-AM, while there was no effect on α7 currents. This suggests that ACh release eliciting α7 nAChR responses is mediated by tight coupling of the presynaptic calcium source and the calcium sensor, while that of α4β2 responses is a looser coupling. Following stimulation of ACh release, there were delayed asynchronous miniature excitatory postsynaptic current (mEPSC) responses. DHβE eliminated both the α4β2 currents and the asynchronous current events. However, MLA eliminated α7 responses but did not impact the asynchronous events, thus confirming that the asynchronous responses were mediated by α4β2 nAChRs. The α4β2 mediated asynchronous activity was also inhibited by EGTA-AM. The spontaneous excitatory postsynaptic activity prior to light stimulation was insensitive to either nicotinic competitive antagonist DHβE or MLA but was inhibited by EGTA-AM and the L-type Ca2+ channel blocker nifedipine.

The substantial reduction in the number of spontaneous events after the application of nifedipine highlights a unique role for L-type calcium channels in regulating spontaneous activity. This could have implications for understanding presynaptic calcium dynamics and spontaneous neurotransmitter release mechanisms.

List of Abbreviation

aCSF	Artificial Cerebrospinal Fluid
α4β2 nAChRs	Alpha 4 Beta 2 Nicotinic Acetylcholine Receptors
α7 nAChRs	Alpha 7 Nicotinic Acetylcholine Receptors
ACh	Acetylcholine
AMPA	α-Amino-3-hydroxy-5-methyl-4-isoxazolepropionic acid
APV	2-amino-5-phosphonovaleric acid
BAPTA-AM	1,2-bis(o-aminophenoxy)ethane-N,N,N',N'-tetraacetic acid, Acetoxymethyl Ester
Ca^{2+}	Calcium Ions
CNQX	6-Cyano-7-nitroquinoxaline-2,3-dione
CNS	Central nervous system
DMSO	Dimethyl Sulfoxide
DHβE	Dihydro-β-Erythroidine
EGTA-AM	Ethylene Glycol-bis(β-aminoethyl ether)-N,N,N',N'-tetraacetic acid, Acetoxymethyl Ester
EPSCs	Excitatory Postsynaptic Currents
GABAA	Gamma-Aminobutyric Acid Type A
GABAergic	Refers to neurons or synapses that release or involve gamma-aminobutyric acid (GABA)
mEPSCs	miniature Excitatory Postsynaptic Currents
IN	Interneuron
LTD	Long-Term Depression
LTP	Long-Term Potentiation
MLA	Methyllycaconitine
mPFC	Medial Prefrontal Cortex
NMDA	N-methyl-D-aspartate
nAChRs	Nicotinic Acetylcholine Receptors
PNS	Peripheral nervous system
PSCs	Postsynaptic Currents
PV	Parvalbumin
RRP	Readily releasable pool
SNc	Substantia Nigra Pars Compacta
SOM	Somatostatin
Syt	Synaptotagmin
TTX	Tetrodotoxin
VGAT	Vesicular GABA Transporter
VAChT	Vesicular Acetylcholine Transporter
VIP	Vasoactive Intestinal Peptide

Acknowledgements

I would like to express my heartfelt appreciation to Dr. Raad Nashmi, my supervisor, for his unwavering support, insightful guidance, and open-door policy that made seeking advice effortless. His daily dedication, spending at least an hour discussing my results, was invaluable to my progress. I am equally grateful to Dr. Kerry Delaney, my first committee member, for his ever-present availability, candid feedback, and constructive criticism, which were instrumental in refining my work. My thanks also go to Dr. Craig Brown, my second committee member, whose foundational teachings in neuroscience greatly enhanced my understanding and who provided guidance during committee meetings.

I am incredibly thankful to my closest friend, Adeeb Akhavan, whose kindness and companionship made this journey much easier. My gratitude also goes to Penny Young, for her valuable comments, support, and consultations during our weekly meetings, and to Keyrian Le Gratiet for his time and valuable advice.

I am deeply grateful to my family. To my father and mother, who have always been there to support and encourage me, and to my sister Danya, who has not only paved the way for me in neuroscience but also supported me daily, both spiritually and academically. To my sister Elnaz, a model of commitment and perseverance, I am inspired by her dedication. Finally, to my brother-in-law James, whose connection with Dr. Nashmi facilitated my path and who created many cherished memories along the way—thank you.

I also extend my gratitude to the University of Victoria for the generous financial support provided through the University of Victoria Graduate Entrance Award, Charles S. Humphrey Graduate Student Award, James A. & Laurette Agnew Memorial Scholarship, and Dr. Julius F. Schleicher Graduate Scholarship. I am also thankful to the Faculty of Science for the Mrs. Annie Greskiw Graduate Award and the SERA award, and to the Department of Biology for the William Wowchuk Memorial Graduate Scholarship.

Contents

List of Figures

Chapter 1. Introduction

1.1 Background and Rationale

Nicotinic acetylcholine receptors (nAChRs) play a crucial role in enhancing cognitive functions (Levin, Petro et al. 2009, Guillem, Bloem et al. 2011), sensory perception (Brown, Sweetnam et al. 2012), and influencing motor activities (Drenan, Grady et al. 2008, Drenan, Grady et al. 2010, Leung, McPhee et al. 2017). These receptors, which are pentameric ligand-gated ion channels, are permeable to the cations Na+, K+, and Ca2+. They rapidly transition to the open state upon binding acetylcholine molecules. While the role of muscle nAChRs in signaling is well-known, the functional significance of neuronal nAChRs in the central nervous system (CNS) remains unclear. Evidence suggests a presynaptic role of neuronal nAChRs in facilitating transmitter release (Mansvelder and McGehee 2000, Zhou, Liang and Dani 2001, Mansvelder, Keath and McGehee 2002, Lambe, Picciotto and Aghajanian 2003, Xiao, Nashmi et al. 2009, Poorthuis, Bloem et al. 2013, Xiao, Miwa et al. 2015), but little is known about the role of postsynaptic nAChR responses in the CNS resulting from acetylcholine release from cholinergic presynaptic terminals (Roerig, Nelson and Katz 1997, Matsubayashi, Amano et al. 2004). The medial prefrontal cortex (mPFC), a critical brain region governing higher cognitive functions, such as motivation and attention (Killcross and Coutureau 2003), has been implicated in disorders like attention deficit hyperactivity disorder and post-traumatic stress disorder (Gamo and Arnsten 2011).

Recent findings indicate the presence of distinct nAChR-mediated currents in the medial prefrontal cortex with varying kinetics (Bennett, Arroyo et al. 2012, Obermayer, Luchicchi et al. 2019), suggesting different presynaptic and postsynaptic mechanisms. The α4β2 nAChR currents in the mPFC exhibit slow and persistent ACh mediated inward currents lasting hundreds of ms (Bennett, Arroyo et al. 2012, Obermayer, Luchicchi et al. 2019), while the α7 nAChR responses rapidly reach their peak response and are transient lasting ~15 ms. These differences in kinetics may indicate unique presynaptic neurotransmitter release mechanisms producing prolonged α4β2 vs α7 responses. Understanding the mechanisms behind the unusually prolonged α4β2 receptor responses in layer 1 mPFC neurons is crucial for unraveling the complexities of neuronal computation and signaling in the CNS.

1.2 Anatomy of the medial prefrontal cortex

The mPFC is a component of the neocortex, which is considered the most recently evolved part of the brain from an evolutionary standpoint. In rodents, the mPFC is comprised of four distinct areas: the medial precentral area (PrCm), the anterior cingulate cortex (ACC), the prelimbic cortex (PLC), and the infralimbic cortex (ILC). These areas can be categorized into two groups based on their connectivity and function: the ventral mPFC (vmPFC) includes the ventral PLC, ILC, and dorsal peduncular cortex, while the dorsal mPFC (dmPFC) comprises the ACC and the dorsal region of the PLC (Heidbreder and Groenewegen 2003, Riga, Matos et al. 2014).

The mPFC in rodents is characterized by its organization into layers and columns, similar to other cortical areas. However, unlike other cortical regions, the rodent PFC is agranular, meaning it lacks layer IV (Poorthuis, Bloem et al. 2013).

1.2.1 Neuronal composition of the medial prefrontal cortex

The mPFC is primarily made up of excitatory pyramidal neurons (approximately 80%) and inhibitory interneurons (around 20%) that have extensive connections with each other (Nieuwenhuys 1994, Rudy, Fishell et al. 2011). Both pyramidal neurons and interneurons can be further categorized based on their cellular characteristics like morphology, physiology, molecular markers, and projection targets, as described by several studies (DeFelipe, López-Cruz et al. 2013, Land, Narayanan et al. 2014, Tremblay, Lee and Rudy 2016). GABAergic neurons, which are predominantly inhibitory, locally target pyramidal neurons and other interneuron types to regulate and synchronize their firing activity. This modulation plays a crucial role in cognitive processes such as attention and goal-directed behavior, as supported by various research findings (Pi, Hangya et al. 2013, Kim, Ährlund-Richter et al. 2016, Tremblay, Lee and Rudy 2016).

The majority of mPFC interneurons can be broadly categorized based on their expression of parvalbumin, somatostatin, or the 5HT3a serotonin receptor (Rudy, Fishell et al. 2011, Tremblay, Lee and Rudy 2016). Another group of interneurons, expressing VIP, represents the largest subset of 5HT3a-positive interneurons (Rudy, Fishell et al. 2011, Tremblay, Lee and Rudy 2016). Fast-spiking (FS) parvalbumin-expressing (PV) and low-threshold spiking (LTS) somatostatin-expressing (SOM) interneurons have specific targets within pyramidal neurons, with parvalbumin and somatostatin interneurons projecting to the soma and dendritic regions, respectively. In contrast, vasoactive intestinal peptide interneurons predominantly project to parvalbumin and somatostatin interneurons (Christophe, Roebuck et al. 2002, Lee, Kruglikov et al. 2013, Pi, Hangya et al. 2013, Karnani, Jackson et al. 2016, Tremblay, Lee and Rudy 2016). Vasoactive intestinal peptide interneurons in the cortex were also found to coexpress ChAT and therefore, are able to cotransmit both GABA and ACh (Obermayer, Luchicchi et al. 2019, Granger, Wang et al. 2020). These interneuron subtypes establish diverse inhibitory microcircuits with other interneurons or pyramidal neurons in the cortex (Lee, Kruglikov et al. 2013, Pi, Hangya et al. 2013, Karnani, Jackson et al. 2016). One type of GABAergic inhibition is feedforward inhibition, where excitatory afferent projections target interneurons which then project to pyramidal neurons (Pouille and Scanziani 2001, Sun, Huguenard and Prince 2006, Adesnik, Bruns et al. 2012). Reciprocal connectivity between pyramidal neurons and interneurons leads to feedback inhibition, influencing the firing activity of pyramidal neurons themselves. Lateral inhibition enables pyramidal neurons to modulate the firing of neighboring pyramidal cells, creating disynaptic inhibitory loops involving PV- or SOM-interneurons (Silberberg and Markram 2007, Berger, Silberberg et al. 2010, Tremblay, Lee and Rudy 2016, Hilscher, Leão et al. 2017). The distinctive spiking behaviors of FS, PV-, and LTS SOM-interneurons produce fast or delayed lateral inhibition, impacting the synchronization of surrounding pyramidal neurons (Silberberg and Markram 2007). Recent research suggests that pyramidal neurons can synchronize neighboring firing activity through delayed lateral inhibition rather than reducing spiking rates (Hilscher, Leão et al. 2017). Coordinated neuronal firing, crucial for sustained attention, may be facilitated by lateral inhibition during attention-demanding tasks (Kim, Ährlund-Richter et al. 2016, Helfrich, Fiebelkorn et al. 2018, Thiele and Bellgrove 2018). Additionally, VIP-interneurons form a unique inhibitory microcircuit by

directly targeting other interneuron types, ultimately disinhibiting pyramidal neurons (Lee, Kruglikov et al. 2013, Pi, Hangya et al. 2013, Karnani, Jackson et al. 2016).

1.2.2 Cholinergic neurotransmission in the mPFC

The activity and functioning of cortical networks are influenced not only by glutamatergic and GABAergic neurotransmission but also by neuromodulators such as acetylcholine (ACh), as highlighted in various studies (Christophe, Roebuck et al. 2002, Bennett, Arroyo et al. 2012, Poorthuis, Bloem et al. 2013, Obermayer, Luchicchi et al. 2019). ACh was the first neurotransmitter discovered by Otto Loewi who observed the action of then coined "vagusstoff" in slowing the frog heart, which was innervated by the cholinergic vagus nerve (Loewi 1924). Later Fatt and Katz (1952) discovered that at the neuormuscular junction of frog skeletal muscle ACh can mediate rapid neurotransmission in the form of excitatory end plate potentials and spontaneous miniature end plate potentials. While many studies emphasize the sustained effects of ACh in the CNS, acting as a slow and nonspecific volume-released neuromodulator that enhances network excitability (Picciotto, Higley and Mineur 2012), recent findings indicate that ACh in the CNS also plays a role in rapid cholinergic point-to-point neurotransmission (Bennett, Arroyo et al. 2012, Estakhr, Abazari et al. 2017, Granger, Wang et al. 2020, Obermayer, Luchicchi et al. 2020, Le Gratiet, Anderson et al. 2022). Cholinergic neurotransmission in the CNS is involved in many cognitive processes include sensory detection, learning, memory, and attention regulation (Dalley, Cardinal and Robbins 2004, Hasselmo 2006, Sarter, Parikh and Howe 2009). The involvement of cholinergic signaling in the mPFC during attention tasks is well-documented (Sarter, Parikh and Howe 2009). Research underscores the significance of ACh in facilitating attention-related cognitive functions. Damage to the cholinergic system results in specific impairments in attention-demanding, goal-directed behavior (Dalley, Cardinal and Robbins 2004). Moreover, an increase in ACh release in the mPFC is observed during correct cue detection, a task reliant on attentional performance (Parikh, Kozak et al. 2007, Sarter, Parikh and Howe 2009). Therefore, the modulation of cortical networks by cholinergic signaling is essential for optimal performance in attention-demanding tasks (Gritti, Manns et al. 2003, Bloem, Schoppink et al. 2014, Zaborszky, Csordas et al. 2015, Ballinger, Ananth et al. 2016).

Acetylcholine is a neurotransmitter that is produced in several tightly clustered nuclei, but has widespread and sparse projections throughout the brain (Woolf and Butcher 2011). The basal forebrain, a brain area composed of several cholinergic nuclei, including the nucleus basalis, the septum, the substantia innominata and the diagonal band of Broca (Mesulam 1995, Zaborszky, Pang et al. 1999, Woolf and Butcher 2011) makes dense cholinergic projections to the cerebral cortex. There are also sparsely distributed cholinergic interneurons of the cortex (Eckenstein and Baughman 1984, von Engelhardt, Eliava et al. 2007). Although ACh production is restricted to a limited number of clustered nuclei in the brain, almost all regions of the brain are innervated by cholinergic neurons and many neurons and glial cells express ACh receptors (Van der Zee and Keijser 2011, Picciotto, Higley and Mineur 2012). In the rat brain, cholinergic neurons in the diagonal band of Broca predominantly innervate the cingulate and occipital cortices. Cholinergic neurons in the substantia innominata target the frontal cortex, while those in the globus pallidus project to

the temporal and parietal cortices (Price and Stern 1983, Rye, Wainer et al. 1984). Within the prefrontal cortex, a frontal-caudal gradient is observed in the location of cholinergic neuron cell bodies in the basal forebrain. Neurons located rostrally, particularly in the horizontal limb of the diagonal band, innervate the rostral and ventral areas of the mPFC, while caudo-lateral neurons, such as those in the substantia innominata and nucleus basalis, preferentially target the dorsal and caudal mPFC regions (Bloem, Schoppink et al. 2014).

Distinct regions within the basal forebrain send cholinergic projections to the neocortex via different pathways (Bloem, Schoppink et al. 2014). Additionally, cholinergic neurons at various locations within the basal forebrain specifically target either superficial or deep layers of the prefrontal cortex(Bloem, Schoppink et al. 2014). Neurons from the rostral basal forebrain project to both superficial and deep layers of the mPFC, whereas those from the caudal regions primarily innervate the deep layers. This indicates the existence of separate populations of basal forebrain neurons that selectively target different layers of the medial prefrontal cortex based on their location within the basal forebrain(Bloem, Schoppink et al. 2014). Overall, cholinergic neurons from diverse basal forebrain regions preferentially innervate specific areas of the medial prefrontal cortex, contributing to the intricacies of cholinergic modulation within cortical networks.

Alongside the long-range cholinergic projections from the basal forebrain, there are also sparse local cholinergic interneurons distributed throughout the cortex (Eckenstein and Baughman 1984). These choline acetyltransferase (ChAT)-expressing interneurons belong to the VIP neuron subclass (Tasic, Menon et al. 2016), with approximately 15% of VIP interneurons coexpressing ChAT (Tasic, Yao et al. 2018). These interneurons exhibit the characteristic bipolar morphology typical of VIP interneurons, with their soma situated in layer 2/3 (von Engelhardt, Eliava et al. 2007).

Activation of these ChAT-VIP interneurons triggers an increase in the frequency of excitatory postsynaptic potentials in pyramidal neurons, a response that is dependent on acetylcholine receptors (von Engelhardt, Eliava et al. 2007) ; and also increase action potential firing in layer 1 interneurons (Obermayer, Luchicchi et al. 2019). Overall, ChAT-VIP interneurons could serve as an additional local source of acetylcholine in the cortex, potentially playing a role in modulating cortical networks during attention-demanding tasks.

The mPFC receives dense cholinergic innervation in all the cortical layers I–III, V and layer VI (Eckenstein, Baughman and Quinn 1988, Poorthuis, Bloem et al. 2013) and it is thought that this neurotransmitter plays an important role in the mPFC, especially in behavior requiring attention (Woolf and Butcher 2011; Obermayer, Luchicchi et al. 2019).

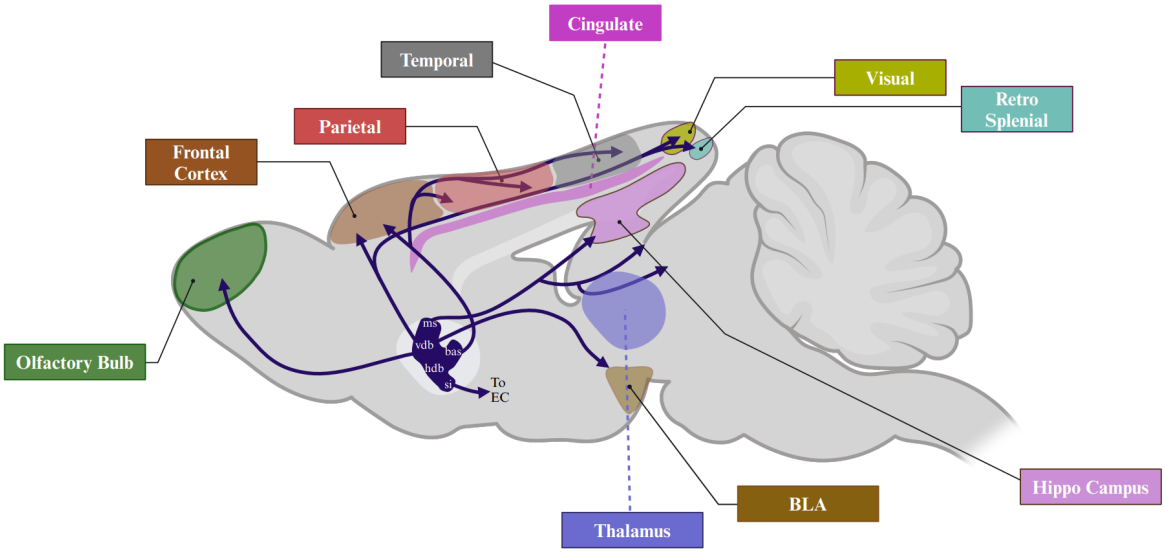

Figure 1-1 Schematic representation of cholinergic projections originating in the basal forebrain.

bas=nucleus basalis, BLA=basolateral amygdala, EC=entorhinal cortex, hdb=horizontal diagonal band nucleus, ms=medial septal nucleus, si=substantia innominate, vdb=vertical diagonal band nucleus. (Adapted from ((Woolf and Butcher 2011).

1.3 Acetylcholine Receptors

ACh signaling is mediated through two major classes of cell-surface receptor proteins: nicotinic ACh receptors (nAChRs) and muscarinic ACh receptors (mAChRs). Nicotinic receptors are ligand-gated ion channels activated by ACh or nicotine, while muscarinic receptors are G protein-coupled receptors activated by ACh or muscarine. Both types of receptors are expressed in the central and peripheral nervous system and are involved in neurotransmission (Gotti, Clementi et al. 2009, Chatzidaki and Millar 2015).

Nicotinic receptors are found on both pre, and post-synaptic neurons and play a role in fast synaptic transmission by allowing the permeation of sodium, potassium, and calcium ions (Gotti, Clementi et al. 2009) down their electrochemical gradient. The mAChR family consists of five subtypes named M1–M5, all of which are expressed in both the CNS and peripheral tissues. The mAChRs are categorized into two functional classes based on their preference for coupling to specific G protein-dependent second messenger pathways (Caulfield, 1993)(Felder 1995). One class includes the M1, M3, and M5 receptor subtypes that primarily couple with the Gq α proteins. This coupling stimulates phospholipase C (PLC), leading to the release of the intracellular second messenger inositol 1,4,5-trisphosphate (IP3). This results in an increase in intracellular calcium levels. The second class comprises the M2 and M4 receptors, which predominantly couple with the Gi/o subtype of G proteins and inhibit adenylate cyclase, leading to a decrease in the second messenger cAMP levels.

1.3.1 Nicotinic acetylcholine receptors

Nicotinic cholinergic synapses in both the central and peripheral nervous systems are intricate molecular structures that share two essential components: acetylcholine as its neurotransmitter and nicotinic acetylcholine receptors. ACh, a small organic molecule synthesized and released

from the cholinergic presynaptic nerve ending, serves as the endogenous neurotransmitter at these synapses. The nAChR is the key component of the postsynaptic apparatus in cholinergic synapses (Zoli, Pucci et al. 2018).

Nicotinic acetylcholine receptors are involved in fast synaptic transmission in the nervous system and also modulate non-excitable cells such as immune cells (Changeux 2012, Zoli, Pucci et al. 2018). nAChRs are composed of five transmembrane subunits, and mammals have sixteen identified subunits, including α1– α7, α9, α10, β1–4, δ, γ, and ε. α8 subunits are only found in birds and α11 and β5 were identified in fish (Pedersen, Bergqvist and Larhammar 2019). Neuronal nAChRs can be assembled as homo-pentamers of α7 or α9 subunits, or as hetero-pentamers of α2–α6 combined with β2–β4 or α9 with α10 subunits. In contrast, muscle nAChRs are hetero-pentamers comprising two α1 subunits and β1, δ, and either a γ (fetal) or ε (post-natal) subunit (Albuquerque, Pereira et al. 2009, Ho, Abraham and Lewis 2020).

In the brain, the most prevalent subtypes of nAChRs are the heteropentameric α4β2 nAChRs (Whiting, Schoepfer et al. 1991, Marks, Pauly et al. 1992), which have high affinity for nicotine and ACh, followed by the homopentameric α7 nAChRs (Clarke, Schwartz et al. 1985), which are highly permeable to calcium and have lower affinity to nicotine and ACh. For homopentameric α7 nAChRs their stoichiometry is denoted as $(\alpha7)_5$, in which the 5 indicates the number of subunits in a receptor. α7 has low affinity to ACh with a EC50 of 272 μM (Briggs and McKenna 1996). α4β2 nicotinic receptors have a high affinity stoichiometry of $(\alpha4)_2(\beta2)_3$ with an ACh EC50 of 1.1 μM and a low affinity stoichiometry of $(\alpha4)_3(\beta2)_2$ with an ACh EC50 of 124 μM (Zwart, Broad et al. 2006).

nAChRs are cation-selective channels that permit the flow of Na+, K+, and Ca2+, leading to membrane depolarization. However, different nAChR subtypes exhibit different conductances and Ca2+ permeabilities (Fucile 2004). The homopentameric α7 nAChR, for example, is highly permeable to calcium, while the addition of the α5 subunit to the heteropentameric α4β2 nAChR significantly increases its calcium conductance (Fucile 2004). Calcium conductance in nAChRs is crucial as it links receptor activation to intracellular signaling pathways (Gubbins, Gopalakrishnan and Li 2010) and mediates the effect of presynaptic nAChR stimulation to increase neurotransmitter release (Dickinson, Kew and Wonnacott 2008).

Although the α4β2 nAChR has lower calcium conductance compared to α7, its activation can still induce intracellular calcium signaling through its interaction with voltage-gated calcium channels (Dajas-Bailador and Wonnacott 2004).

The α7 nAChRs are known to enhance cognitive behaviors such as attention (Young, Crawford et al. 2007, Sydserff, Sutton et al. 2009) and memory (Thomsen, Hansen et al. 2010, Yang, Paspalas et al. 2013). Dysfunction of α7 nAChRs have been linked to various nervous system disorders, including altered expression in smokers' brains, individuals with schizophrenia, and Alzheimer's disease (Wevers, Monteggia et al. 1999, AhnAllen 2012). In the mPFC, β2*-nAChRs are found postsynaptically on cells, with a strong presence of α4β2α5 nAChRs on pyramidal cells in layer VI and α4β2* nAChRs (* indicates the possible presence of other nAChR subunits) on interneurons in all layers (Poorthuis, Bloem et al. 2013). Studies have shown significantly reduced levels of cortical α4β2 nAChRs in Alzheimer's disease patients (Sparks, Beach and Lukas 1998, Perry, Martin-Ruiz et al. 2000).

These findings underscore the critical role of nAChRs in cognitive function and their implications in various neurological disorders.

1.3.2 Nicotinic receptor expression in the medial prefrontal cortex

Researchers demonstrated that nAChRs-mediated modulation in the mPFC is specific to particular layers (Poorthuis, Bloem et al. 2013). This research also clarified the differences in nicotinic modulation between pyramidal cells and interneurons, systematically exploring the subunit composition of nAChRs expressed in these neuronal classes across different layers. Soon after, it was confirmed that the layer-specific diversity of nAChRs in the PFC is crucial for functional control of cortical processing and plasticity (Verhoog, Obermayer et al. 2016).

The rodent mPFC exhibits specific nAChR isoforms across different neuron types and layers. The two main nAChR isoforms in the mPFC are homomeric α7 nAChRs and heteromeric α4β2* nAChRs. Research indicated that α7 nAChRs are found on interneurons in layers I, II/III, and V, as well as on a small number of pyramidal neurons in layer II/III and the majority of pyramidal neurons in layer V. Meanwhile, α4β2 nAChRs are present on thalamocortical glutamatergic terminals in layer V, fast-spiking interneurons in that same layer, non-fast-spiking interneurons across all layers, and pyramidal neurons in layer VI exclusively (Patel, Nguyen et al. 2023).

The homopentameric α7 nAChRs and heteropentameric α4β2* nAChRs have distinct functional properties and are expressed differently among various neuronal types and within cellular layers of the mPFC (Abbondanza, Urushadze et al. 2024). Homopentameric α7 nAChRs are characterized by low acetylcholine sensitivity, high calcium permeability, rapid kinetics, and quick desensitization (Gotti, Zoli and Clementi 2006, Dani and Bertrand 2007). In contrast, heteropentameric α4β2 nAChRs demonstrate slower activation kinetics and higher sensitivity to acetylcholine. The function of heteromeric nAChRs also varies depending on the subunit occupying the accessory position (Wang, Kuryatov et al. 2015, Jain, Kuryatov et al. 2016, Wang and Lindstrom 2018).

In layer I neurons, the mRNAs of α4β2, and α7-nAChR subunits are predominantly expressed (Christophe, Roebuck et al. 2002). Studies have shown that the selective antagonists of α4β2 or α7 nAChR can inhibit the enhancement of neuronal excitation by nicotine in these neurons (Christophe, Roebuck et al. 2002, Chen, Xiong and Yan 2013), indicating that both receptor subtypes mediate the nicotinic regulation of neuron activity in layer I.

Layer I of the mPFC stands out for its unique composition, devoid of excitatory neuron cell bodies. Instead , layer I is populated by a specialized group of GABAergic interneurons (Schuman, Machold et al. 2019), with distinct subtypes expressing serotonin receptor 5HT3a and the α7 nicotinic subunits (Schuman, Dellal et al. 2021),(Schuman, Machold et al. 2019). These α7 containing cells, with notable characteristics like large cell bodies and multipolar dendrites, account for around 20% of the GABAergic population in layer I (Schuman, Dellal et al. 2021). Recent studies in the medial prefrontal cortex have highlighted the connectivity between these GABAergic neurons and cholinergic neurons in from deeper layers, revealing modulatory responses mediated by nAChRs (Obermayer, Luchicchi et al. 2019).

In the medial prefrontal cortex, the modulation by nAChRs varies across different layers, Typically, this modulation results in inhibitory outputs in layers II/III, while layers V

and VI experience an overall increase in neuronal activity (Poorthuis, Bloem et al. 2013). In studies of recordings of layer I, II and III interneurons of the mPFC it was shown that stimulating long range projections from the basal forebrain fibers (Arroyo, Bennett et al. 2012) or stimulation of cortical cholinergic interneurons (Obermayer, Luchicchi et al. 2019) triggers both rapid and slow nicotinic responses in layers I and II/III, with the rapid response mediated by α7 nAChRs, while the slow response was mediated by α4β2 nAChRs (Arroyo, Bennett et al. 2012). The α7 nicotinic responses were rapid, transient, and sensitive to the antagonist MLA, while the α4β2 nicotinic responses, built up slowly over hundreds of milliseconds and were sensitive to the inhibitor DHβE (Arroyo, Bennett et al. 2012).

It is proposed that these two types of nicotinic responses may arise from distinct synaptic mechanisms, possibly indicating differences between phasic synaptic and extrasynaptic volume ACh transmission (Parikh, Kozak et al. 2007, Arroyo, Bennett et al. 2012). The complexity of cholinergic transmission in the prefrontal cortex is not fully understood, with rapid and slow nicotinic responses observed due to different nAChR subtypes. This intricate modulation is influenced by factors like subcellular localization of postsynaptic nAChRs and presynaptic ACh release sites.

1.4 Synchronous, asynchronous and spontaneous neurotransmitter release

The remarkable ability of the brain to perform a wide array of functions is rooted in the capacity of neurons to communicate at synapses. The transmission of signals between neurons occurs through synaptic transmission, where specialized structures known as synapses facilitate the process. In this setting, an activated presynaptic neuron releases neurotransmitter molecules into a narrow gap, the synaptic cleft, where they diffuse and bind to ligand-gated ion channels or G protein coupled receptors on the postsynaptic neuron. The activation of these receptors conveys the synaptic message as electrical currents and initiates intracellular signaling cascades. Synapses are the fundamental units of neurotransmission, characterized by their small size (~1 μm^2) and a narrow synaptic cleft (~15 nm), which allows for the rapid diffusion of neurotransmitters from the presynaptic terminal to the postsynaptic receptors, triggering a response in a millisecond or less (Goyal and Chaudhury 2013, Tang, Chen et al. 2016).

Neurotransmitter release operates predominantly through three modes: synchronous release, which occurs within a millisecond following an action potential at the presynaptic bouton; asynchronous release, which can last from tens of milliseconds to several seconds post-action potential; and spontaneous release, which occurs without presynaptic depolarization. The arrival of an action potential at the axon terminal initiates neurotransmitter release via a rapid increase in calcium concentration in the presynaptic bouton —termed calcium nanodomains—leading to a synchronized fusion of synaptic vesicles (Neher and Sakaba 2008). This synchronous release is critical for quick neurotransmission. Additionally, synaptic vesicles may continue to fuse asynchronously or in a delayed fashion after the action potential for variable durations (tens of ms to seconds), influenced by factors such as neuron type, developmental stage, and previous activity history (Kaeser and Regehr 2014, Jiang, Yang et al. 2015, Luo, Bacaj and Südhof 2015). The extent and timing of this asynchronous release are modulated by calcium influx and the buffering capacity of presynaptic terminals (Neher and Sakaba 2008), along with the inherent

characteristics of the neurotransmitter release machinery. In contrast, spontaneous neurotransmitter release occurs independently of neuronal activity and is subject to variable regulation by calcium levels (Kavalali 2015). The three modes of neurotransmitter release were initially identified and characterized functionally using electrophysiological methods; however, it later became clear that the molecular characteristics of synaptic vesicles play a significant role in this diversity (Südhof 1995).

From a functional standpoint, synaptic vesicles can be classified by their tendency to fuse. The readily releasable pool (RRP) consists of the first vesicles that fuse in response to stimulation, indicating a high propensity for fusion (Kaeser and Regehr 2017). The RRP exhibits a strong correlation between its function and morphology (Zenisek 2008, Mehta, Snellman et al. 2013), as seen in sensory neuron synapses, where the number of docked vesicles reflects the fast, synchronous release triggered by stimulation, while vesicles situated away from the ribbon may fuse spontaneously (Zenisek 2008). In smaller central synapses, such as those in the hippocampus, the size of the RRP correlates with the number of docked synaptic vesicles at the active zone, with the regulation of active zone size and the number of docking and release sites affecting release probability and synaptic strength (Murthy, Schikorski et al. 2001, Michel, Müller et al. 2015, Rey, Smith et al. 2015). The reserve pool of vesicles can also merge with the RRP during mild to prolonged stimulation, aiding in the maintenance of neurotransmission (Sara, Mozhayeva et al. 2002, Marra, Burden et al. 2012). The sizes of the RRP and the reserve pool are variable among synapses, approximately they occupy ~0.5% and ~10–60% of the total pool, respectively (Marra, Burden et al. 2012, Guo, Ge et al. 2015, Qiu, Zhu and Sun 2015). Together, the RRP and reserve pool form the recycling pool of synaptic vesicles, while the remaining vesicles constitute what is known as the “resting” or “dormant” pool, which is less responsive to activity) (Südhof 2000, Fredj and Burrone 2009, Guo, Ge et al. 2015).

Recent advancements and previous findings have led to a plausible model for how key proteins facilitate neurotransmitter release. In this model, SNARE (soluble N-ethylmaleimide-sensitive factor attachment protein receptor) proteins—syntaxin-1, synaptosomal-associated protein (SNAP)-25, and synaptobrevin—form tight complexes that bring the membranes together, playing a crucial role in membrane fusion. Soluble N-ethylmaleimide-sensitive factor (NSF) and SNAPs then disassemble these SNARE complexes, ensuring that fusion occurs through a finely regulated pathway, initiated by Munc18-1 binding to a 'closed' conformation of syntaxin-1. This complex also anchors synaptobrevin, allowing for SNARE complex assembly when Munc13-1 opens syntaxin-1, linking the vesicle and plasma membranes. Synaptotagmin-1 and complexin bind to the partially assembled SNARE complexes, likely stabilizing them until calcium binding to synaptotagmin-1 causes it to dissociate from the complex, promoting interactions with phospholipids that trigger neurotransmitter release. Although significant questions remain regarding the precise mechanism of membrane fusion, these insights offer a framework to explore the mechanisms underlying presynaptic plasticity (Rizo 2022).

The synaptotagmin (Syt) family of molecules, an evolutionarily conserved family of proteins, is known for regulating calcium-dependent membrane fusion events. Mice and humans express 17 synaptotagmin isoforms with differential expression patterns across

tissues and cell types. All 17 Syts are expressed in the brain, and eight of them (Syt1, 2, 3, 5, 6, 7, 9 and 10) bind Ca2+ and regulate vesicle fusion (Wolfes and Dean 2020, Zhou 2023).

Synchronous neurotransmitter release is driven by fast synaptotagmin isoforms, including Syt1, Syt2, and Syt9 (also known as Syt5). These synaptotagmins exhibit the lowest Ca2+ affinity (EC50 = 10–20 μM), and they detect local Ca2+ increases from nearby calcium channels, which open in response to action potentials (Sugita, Shin et al. 2002, Xu, Mashimo and Südhof 2007, Eggermann, Bucurenciu et al. 2011).

In contrast, although asynchronous release also depends on Ca2+, it utilizes a different mechanism and Ca2+ source than synchronous release. High-affinity Ca2+ sensors specifically regulate asynchronous release by responding to bulk cytosolic Ca2+ fluctuations rather than localized Ca2+ microdomains. Syt7, with its tenfold higher Ca2+ affinity (EC50 = 1–2 μM) and slower kinetics compared to Syt1, is hypothesized to mediate asynchronous release (Sugita, Shin et al. 2002, Otsu, Shahrezaei et al. 2004).

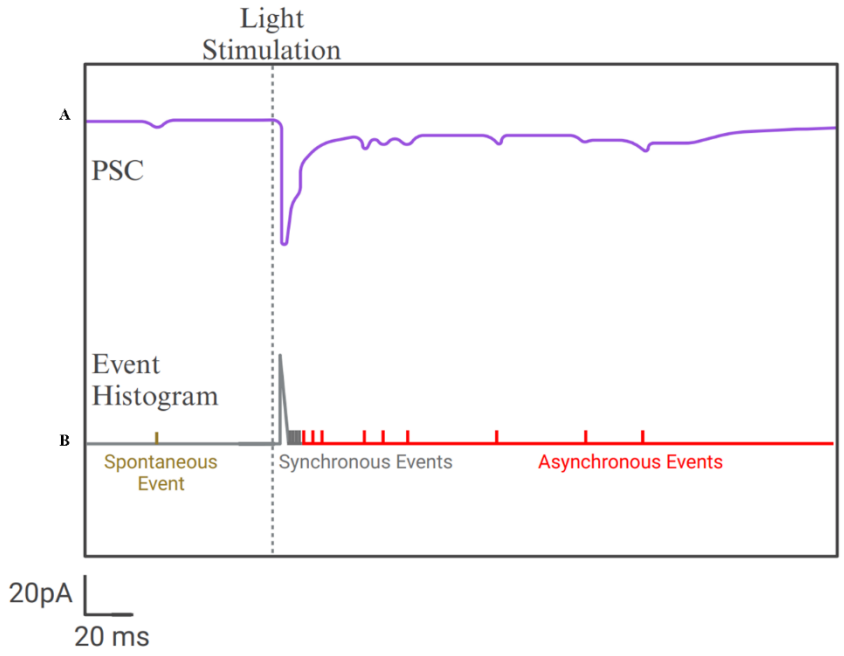

Figure 1-2 Different types of synaptic transmission illustrated with simulated data.
(a) Stimulation evokes synchronous and asynchronous release. (b) Spontaneous neurotransmitter release is shown on a different timescale. Abbreviations: PSC, postsynaptic current. Adapted from(Kaeser and Regehr 2014)

1.5 Research Objectives and Hypothesis

This study will examine the different properties of acetylcholine release driving α7 versus α4β2 nicotinic responses in layer 1 neurons of the medial prefrontal cortex.

Furthermore, I aim to investigate the different mechanisms mediating ACh release between α7 versus α4β2 synapses, focusing on the strength of coupling between calcium sensors and calcium channels in presynaptic terminals. This thesis aims to characterize and provide understanding of the mechanisms that lead to these prolonged α4β2 responses and

asynchronous synaptic activity. Asynchronous neurotransmitter release can result from various factors, including changes in calcium influx and the dynamics of synaptic vesicle release (Kaeser and Regehr 2014).

Specifically, I will assess how tightness of coupling between calcium source and sensor differs for α7 versus α4β2 synapses and whether presynaptic L-type Ca2+ channels, which inactivate slowly, or a presynaptic muscarinic receptor with slow kinetics may mediate the persistent kinetics of the slow α4β2 nAChR currents.

Chapter 2.
Materials and Methods

2.1 Animal Care and Breeding

All animal experiments were conducted in adherence to the animal care protocols sanctioned by the University of Victoria Animal Care Committee and in accordance with the guidelines established by the Canadian Council on Animal Care (CCAC). Mice were bred and housed in the University of Victoria Animal Care Unit (UVic ACU) where they were subjected to a regulated 12-hour light/dark cycle and provided with unlimited access to food and water.

The mouse strain used in this research was the ChATcre::ChR2(H134R)-eYFP strain, which was bred to homozygosity for both genes through breeding crosses between the ChATcre (neodel) strain (JAX stock# 031661) and the ChR2(H134R)-eYFP mice (JAX stock# 012569). ChATcre (neo-del) is a knock-in mouse line in which cre-recombinase was inserted into the choline acetyltransferase (ChAT) promoter and the frt flanked neomycin resistance selection gene was removed with flip recombinase. The ChR2(H134R)-eYFP mice are knock-in mice in which channelrhodopsin2-YFP with the H134R variant was inserted in the promoter region of the Rosa26 locus. Offspring from this crossbreeding express channelrhodopsin2 (ChR2) fused with yellow fluorescent protein (eYFP) in cholinergic neurons.

2.2 Brain Slice Preparation for Electrophysiology

In this research, coronal brain slices were prepared from ChATcre::ChR2(H134R)-eYFP knock-in mice aged 22 to 36 days. The mice were deeply anesthetized with isoflurane, intracardially perfused with cold and carbogen bubbled N-methyl-D-glucamine (NMDG)-based cutting solution and swiftly decapitated. NMDG is an organic cation and when ion substituted for sodium is known to diminish ion permeation through sodium channels. This property helps improve neuronal viability as compared to sucrose substituted aCSF during brain sectioning (Ting et. al, 2014).

After the brain was removed, it was placed in ice-cold, carbogen-bubbled NMDG-based cutting solution for 1 min. The brain was embedded in 3% agar-A (CAS #9002-18-0, Bio Basic Canada) at a temperature range of 37–38°C and chilled on ice. Once the agarose solidified it was glued on the vibratome cutting platform and coronal sections of 320 μm thickness were sliced using a Leica VT 1000S vibratome, targeting the prefrontal cortex.

Following slicing, the brain slices underwent an initial recovery period of 10 min in NMDG-based cutting solution at 32–34°C. The use of NMDG is crucial as it replaces sodium present in standard aCSF to prevent sodium influx and block action potentials. This substitution provides a protective phase for brain cells immediately after slicing, stabilizing the membrane potential and preventing excitotoxicity without the energy demands associated with continuous synaptic activity. In addition, NMDG promotes neuronal viability, reduces cellular edema, and preserves synaptic function during the recovery phase.

To eliminate any residual NMDG, the brain slices were rinsed with oxygenated artificial cerebrospinal fluid (aCSF) before being transferred to a chamber containing room temperature aCSF. Subsequently, the slices were incubated for 15 min in aCSF at room temperature. Throughout the post-slicing process, the brain sections were shielded from light to prevent potential activation of channelrhodopsin-expressing cells.

2.3 Solutions Used

NMDG-Based Cutting Solution: Developed to safeguard brain tissue integrity during slicing procedures, this cutting solution replaces sodium with NMDG. The composition of the cutting solution includes 92 mM NMDG, 2.5 mM KCl, 1.25 mM NaH_2PO_4, 30 mM $NaHCO_3$, 20 mM HEPES, 25 mM D-glucose, 5 mM Na-ascorbate, 3 mM Na-pyruvate, 0.5 mM $CaCl_2$, and 10 mM $MgCl_2$, with a pH of 7.3.

Artificial cerebrospinal fluid (aCSF): Following the initial NMDG-based recovery phase, the brain slices were shifted to freshly prepared aCSF. aCSF contained: 118 mM NaCl, 2.5 mM KCl, 1.25 mM NaH_2PO_4, 24 mM $NaHCO_3$, 12.5 mM D-glucose, 3 mM Na-ascorbate, 1.5 mM Na-pyruvate, 2 mM $CaCl_2$, and 1 mM $MgCl_2$. A rinse with aCSF removed any residual NMDG after the NMDG incubation before the final recovery phase. The slices were maintained in room temperature aCSF for 15 minutes post-rinsing prior to electrophysiological recordings.

2.4 Electrophysiological Recordings

The brain slice was positioned in the recording chamber and neurons were visualized using an upright Nikon FN1 microscope system equipped with a CFI APO 40X W NIR objective (water immersion, 0.8 numerical aperture, 3.5 mm working distance). Continuous perfusion of carbogenated aCSF was maintained in the chamber at 31°C by a dual-channel temperature regulator (Warner Instruments, cat# TC-344C).

Visualization of layer 1 interneurons in the medial prefrontal cortex (the prelimbic area (PL) in the medial prefrontal cortex which corresponds to a Bregma position of approximately +1.70 mm to +2.20 mm) was achieved using a Thorlabs Kiralux CMOS camera (CS505MU) under infrared differential interference contrast (IR-DIC) illumination. Whole-cell patch-clamp recordings were conducted with borosilicate glass electrodes (4-6 MΩ resistance, cat# 1B150F-4, World Precision Instruments) filled with internal pipette solution comprised of 125 mM Cs-gluconate, 2 mM TEABr, 2 mM $MgCl_2$, 10 mM HEPES, 0.5 mM $CaCl_2$, 5 mM EGTA, 5 mM phosphocreatine Tris, 3 mM Mg-ATP, 0.2 mM GTP Tris, 5 mM QX-314Br, and 2 mM L-glutathione, titrated to pH 7.4 (295 mOsm). Reversal potentials for this solution were ECl = -55 mV and GHK = -30 mV.

Recordings were done in voltage-clamp mode and cells were held near their calculated Goldman-Hodgkin-Katz potential at -30 mV before transitioning to -60 mV for each sweep of the recording. At the near start of the sweep a -5 mV 50 ms step was performed to continually assess the access resistance.

All recordings were amplified with a MultiClamp 700B amplifier (Molecular Devices) and low pass Bessel filtered at 10 kHz. The data were digitized at a sampling rate of 20 kHz via a Digidata 1440A A/D board (Molecular Devices) and recorded using pCLAMP 10.6 acquisition software (Molecular Devices). Recordings were done in voltage-clamp mode and cells were held near their calculated Goldman-Hodgkin-Katz potential at -30 mV before transitioning to -60 mV for each sweep of the recording. The holding potential was corrected for the liquid junction potential, which was calculated to be -13 mV. Pipette and cell membrane capacitances were corrected along with a 40% correction applied to the series resistance.

2.5 LED Light Stimulation

Activation of channelrhodopsin2 was carried out using a collimated LED integrated into the microscope setup, transmitting light through a CFI APO 40X W NIR objective (water immersion, 0.8 numerical aperture, 3.5 mm working distance). The LED had a peak wavelength of emission of 470 nm (Thorlabs, M470L3-C5) specifically selected for activating channelrhodopsin in optogenetic experiments.

Light intensity was controlled using an LED driver (Thorlabs LEDD1B), which received an analogue voltage pulse signal from the Digidata 1440A A/D converter driven by pCLAMP software. The power density of the 470 nm LED light was calibrated using a photometer (PM100USB, Thorlabs) and set to 20 mW/mm² with a 5 ms pulse duration. The onset and duration of LED illumination were monitored using a photodiode positioned into the light path of the LED upstream of the objective, recorded with pCLAMP software simultaneously while LED evoked voltage-clamp currents were recorded from the layer 1 neuron. The LED illumination field was a diameter of 560 μm.

2.6 Pharmacology

In the experiments CNQX (10 μM) and D-APV (20 μM) were introduced into the bath solution to inhibit AMPA/kainate and NMDA receptors, respectively. Moreover, gabazine (SR 95531 hydrobromide) (10 μM) or bicuculline (10 μM) was utilized to inhibit $GABA_A$ receptors.

To explore the involvement of nicotinic receptors, the competitive antagonists DHβE (1 μM) and MLA (10 nM) were applied to selectively inhibit α4β2 and α7 nicotinic receptors, respectively.

EGTA-AM (100 μM) was employed to differentiate between loose and tight coupling between the calcium sensor and the calcium channel at presynaptic terminals. With its slower calcium-binding kinetics, EGTA enables researchers to probe synaptic mechanisms where calcium channels and sensors are spatially separated, revealing loose coupling interactions. As a control, BAPTA-AM (30 μM), which binds calcium more rapidly than EGTA, was used to evaluate tight coupling in synapses where rapid calcium buffering is crucial for neurotransmission.

Nifedipine (1 μM), an L-type calcium channel blocker, was utilized to evaluate the role of these channels in calcium dynamics during neurotransmission. Atropine (500 nM), a muscarinic acetylcholine receptor antagonist, was introduced to investigate the impact of G-protein-coupled receptors (GPCRs) on the recorded responses.

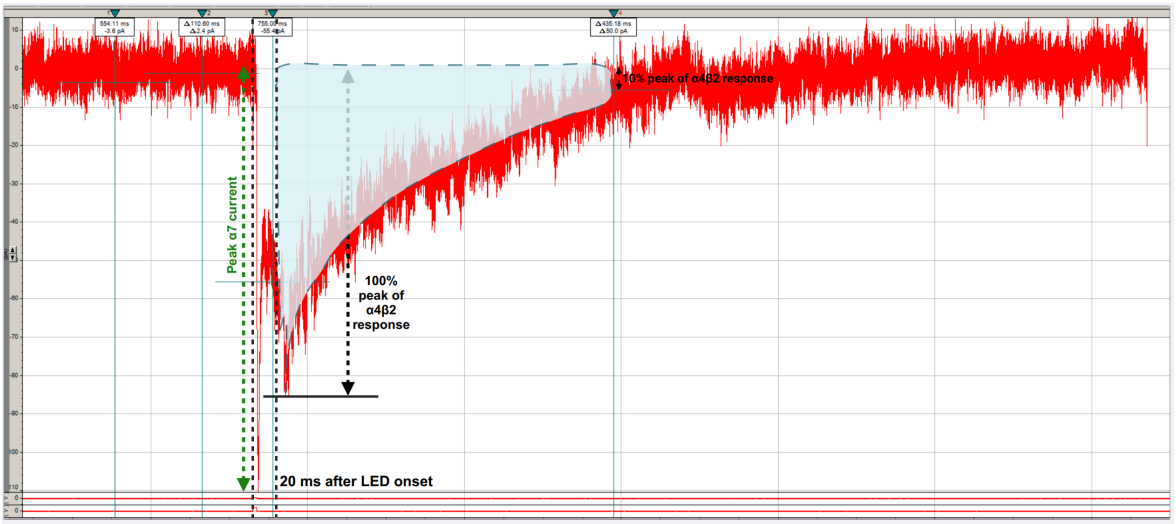

Figure 2-1 Measurement of α4β2 Area Under the Curve Using Clampfit
To quantify the area under the curve for α4β2 nicotinic receptor responses, we analyzed electrophysiological recordings using Clampfit 10.7 (Molecular Devices). The measurement window begins 20 ms after LED onset, as α7 receptor responses have fully decayed by this point, ensuring that the calculated area reflects pure α4β2 activity without contamination from α7-mediated currents. The area under the curve is determined between this 20 ms mark and the time point when the α4β2 response reaches 10% of its peak amplitude. The recorded traces were baseline-subtracted before analysis, and cursor placements were kept consistent across all stimulation sweeps for each recorded cell.

2.7 Analyses of Electrophysiological Data

2.7.1 Analyses of Kinetic Properties of Nicotinic Currents Including Latency to Onset, Time to Peak and Decay Times

To detect the latency to onset of synchronous events, we used Clampfit version 10.7. Baseline holding currents were adjusted to zero through baseline subtraction during the baseline time period just before the evoked response. Traces were processed with a high-pass Bessel filter at 30 Hz and a low-pass boxcar filter smoothed over 31 points. The two cursors were placed such that one was positioned at 2 ms post-LED stimulation and the second cursor was positioned 20 ms after the onset of the LED light stimulation. To determine the time of onset of the synchronous synaptic event, we used the event detection function in Clampfit using a threshold set at -3 pA, which was a value which was approximately two times the standard deviation of the zeroed baseline current value before the LED stimulation. The latency to onset of the synchronous response was calculated to be the time of the synchronous event minus the time of the onset of the LED stimulation. Onset times for α4β2 currents were done in the presence of the α7 nAChR inhibitor MLA and onset times for α7 nicotinic receptor currents were done in the presence of the α4β2 nAChR inhibitor DHβE.

Time to peak was determined using the 10% to 90% rise time function in Clampfit and decay time was determined using the 90% to 10% decay time function in Clampfit.

2.7.2 Peak Current Amplitude of α7 and Area Under the Curve (Charge) for α4β2 Nicotinic Cholinergic Responses

For peak current amplitude detection, we used Clampfit version 10.7 to place cursors for capturing the maximum current response amplitude. First, baseline holding currents were adjusted to zero through baseline subtraction during the baseline time period just before the evoked response. Cursor 1 and cursor 2 were positioned on the baseline prior to LED stimulation as the reference region. Cursor 3 was placed at the onset of LED light stimulation and cursor 4 was set at 20 ms post-LED onset to ensure the recorded peak specifically reflected synchronous α7 receptor activity, as α7 receptors typically decayed to baseline within this time frame.

To measure the area under the current or charge for α4β2 responses, first the baseline holding currents were adjusted to zero through baseline subtraction during the baseline time period just before the evoked response. Cursors 1 and 2 were positioned on the baseline prior to LED stimulation as the reference region. Then the area was determined between two set cursors 3 and 4 with cursor 3 set at 20 ms after the onset of LED since α7 responses returned back to baseline by around 15 ms and the cursor 4 was positioned at the time when the α4β2 current decayed to 10% of the peak amplitude of the α4β2 current. These two cursor positions were kept constant for all subsequent LED stimulation sweeps for the recorded cell (Figure2-1).

2.7.3 Event Detection for Asynchronous Events Using the Thresholding Procedure

Data processing was conducted using Clampfit version 10.7. First, baseline holding currents were adjusted to zero through baseline subtraction during the baseline time period just before the evoked response. The raw current traces underwent filtering with a low-pass boxcar filter set to a smoothing of 31 points. Next, a high-pass Bessel filter with a cutoff frequency of 30 Hz was applied to filter out the slow α4β2 current to better isolate the transient asynchronous events. We used the event detection function in Clampfit using a threshold set at -3 pA, which was a value which was approximately two times the standard deviation of the zeroed baseline current value before the LED stimulation. Finally, the times of the detected events were transferred into a spreadsheet for further analysis.

2.7.4 Analysis of Asynchronous Activity by Taking the Area Under the Square Root of α4β2 Current Response Squared

We used a second method to analyze the asynchronous activity to corroborate our findings using the event thresholding detection method. Using Clampfit 10.7, baseline holding currents were adjusted to zero through baseline subtraction during the baseline time period just before the evoked response. The raw current traces underwent filtering with a low-pass boxcar filter set to a smoothing of 31 points. Next, a high-pass Bessel filter with a cutoff frequency of 100 Hz was applied to filter out the slow α4β2 current to better isolate the transient asynchronous events. The filtered current traces were then put through a transform in which the current was squared and then the square root was taken. Using the "Arithmetic" function under the "Analyze" tab in Clampfit, we applied the square root function with the expression (t1..n = sqrt((t1..n)^2) where n denotes the last selected sweep in the series, sqrt

denotes the square root transform and ^2 denotes raising to the second power. Then the area under the curve of the resultant filtered and transformed traces was taken between the cursors placed at 20 ms after the onset of the LED and at 1120 ms after the onset of LED stimulation. We also determined the pre-stimulus baseline activity area with two cursors positioned on the trace before the LED stimulation. To calculate the final asynchronous activity the baseline pre-LED stimulation area was multiplied by a factor to equal the length of time between the cursors post-LED stimulation and subtracted from the area under the curve between the cursors for the post-LED stimulation. We analyzed asynchronous activity by these two different approaches to increase our confidence in the accuracy of our asynchronous event analysis, especially in experiments testing the effects of EGTA, BAPTA, DMSO, and non-DMSO conditions. Schematic procedures for the Square Root Squared Transform Analysis is depicted in Figure 2-2.

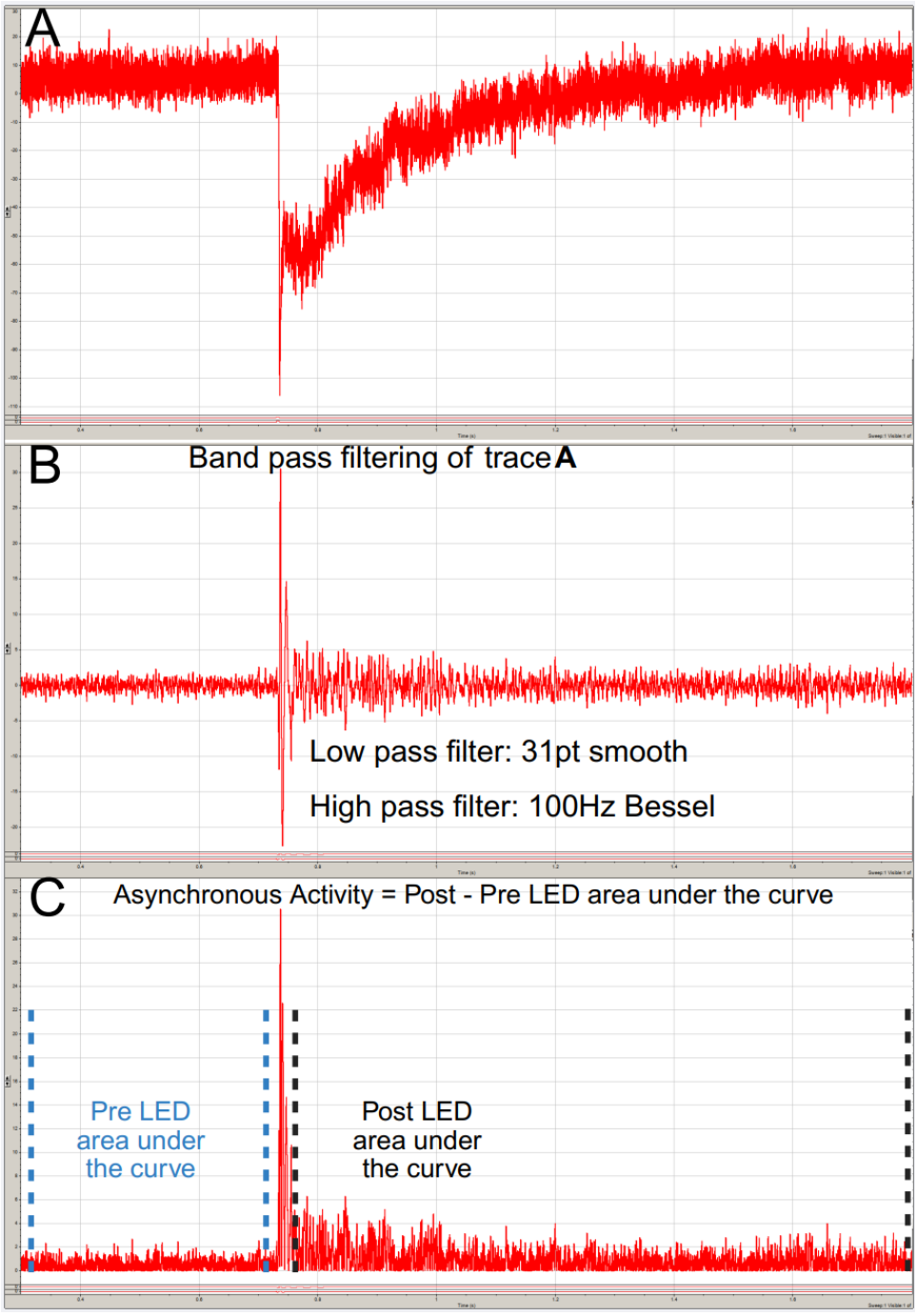

Figure 2-2 Schematic procedure for Square Root Transform Analysis.
We used Clampfit version 10.7 for data processing. First, the raw data were filtered using a low-pass filter (type: boxcar) with a smoothing frequency of 31 Hz. Subsequently, a high-pass filter (type: Bessel, 8-pole) with a 100 Hz cutoff was applied to isolate asynchronous event characteristics. Following filtering, we selected the sweep data for square root analysis. Using the "Analyze" tab in Clampfit, we applied the square root function with the expression $(t1..n=\sqrt{(t1..n)^2}$)where n denotes the last selected sweep in the series. Finally, to quantify the data, we calculated the area under the curve (Charge) of the transformed (square root) data, utilizing the statistical functions available in the "Analyze" tab of Clampfit. This additional square root analysis method complements event detection and Charge calculations, ensuring a robust assessment of asynchronous events in α4β2 responses under various experimental conditions.

2.8 Statistical Analyses

Values were presented as mean ± standard error of the mean (SEM). Electrophysiological traces were plotted with Igor Pro software. Electrophysiological recordings were analyzed with pClamp software. Graphs were plotted using Prism 10.2.0 (GraphPad). Statistics were performed using R (v4.0.3, 2020) or Prism 10.2.0 (GraphPad).

The normality of the data was assessed using either the Shapiro-Wilk test or the Kolmogorov-Smirnov test. Equal variances were assessed using a Fligner-Killeen test of homogeneity of variances. If parametric assumptions were passed a t test comparison was performed on two independent samples of data or a paired t test for two related measurements over the same neurons. Otherwise the nonparametric Wilcoxon sum rank test or the Wilcoxon signed rank test were performed, respectively.

Chapter 3.
Results

3.1 Kinetic and Pharmacological Properties of Cholinergic Mediated Nicotinic Acetylcholine Receptor Currents in Layer 1 Medial Prefrontal Cortical Neurons

To confirm that the pharmacologically isolated nicotinic responses were exclusively comprised of α7 and α4β2 nAChRs, I used specific nAChR antagonists in the presence of a pharmacological cocktail that effectively inhibited NMDA receptors with APV (20 μM), AMPA receptors with CNQX (10 μM), and $GABA_A$ receptors with gabazine (10 μM).

Following the establishment of stable whole-cell patch-clamp recordings from layer 1 medial prefrontal cortical neurons, optogenetic stimulation of ACh release elicited nicotinic acetylcholine receptor mediated currents. The nicotinic currents had two components with vastly different kinetic properties as has been described previously (Bennett, Arroyo et al. 2012, Obermayer, Luchicchi et al. 2019).

The α7 nAChR competitive anatagonist MLA (10 nM) resulted in a significant reduction in peak response amplitude of the rapid transient inward current, indicating effective α7 receptor inhibition ($W = -15.00$, $p = 0.031$, $n = 5$) (**Fig. 3-1B, C)**. Meanwhile, α4β2 competitive antagonist DHβE (10 μM) significantly eliminated the slow and persistent α4β2 nicotinic current (**Fig. 3-1A, D)** ($W = -15.00$, $p = 0.031$, $n = 5$). The "apparent" nonsignificant decrease in α7 current with DHβE was due to the fact that the onset of α4β2 receptors was no different than α7 (**Fig. 3-1E,H**), so DHβE abolished the α4β2 current that overlapped temporally with α7.

When analyzing the kinetic response characteristics of α7 and α4β2 receptors, we observed that α7 had a significantly shorter time to peak compared to α4β2 (2.1 ± 0.1 ms vs 62.7 ± 9 ms, respectively) ($t(10) = 20.8$, $p < 0.0001$, $n = 10$ neurons per group) (**Fig. 3-1F**). α7 also exhibited a markedly shorter time to decay than α4β2 receptors (7.4 ± 0.6 ms vs 497 ± 37 ms, respectively) ($t(9.00) = 13.3$, $p < 0.0001$, $n = 10$ per group) (**Fig. 3-1G**) but no significant difference in response onset between α7 and α4β2 receptors ($t(17.8) = 0.02$, $p = 0.49$, $n = 10$ neurons per group) (**Figure 3-1E,H**).

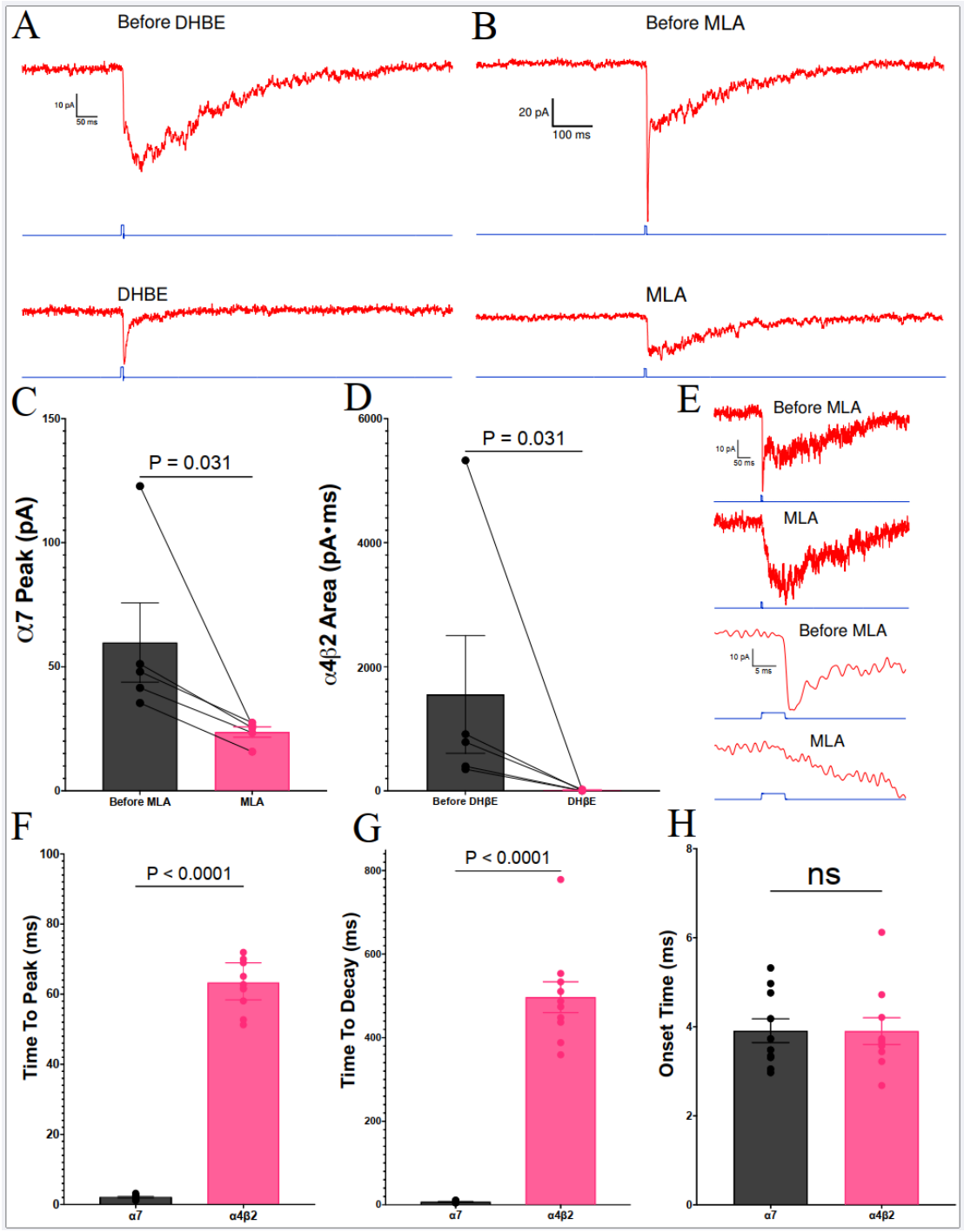

Figure 3-1 Pharmacological sensitivity of α7 and α4β2 nicotinic receptors and their kinetic properties. Application of DHβE (10 μM) significantly eliminated the slow and persistent α4β2 (**A**, **D**), while MLA (10 nM) reduced the α7 peak amplitude (**B**, **C**), indicating effective α7 receptor inhibition. DHβE also slightly decreased the α7 peak, likely due to temporal overlap between α4β2 and α7 responses. Kinetic analyses of α7 nAChRs were performed in the presence of DHβE while those of α4β2 were done in the presence of MLA. Kinetic analysis revealed that α7 nAChRs exhibited a significantly shorter time to peak (2.1 ms vs 62.7 ms) and time to decay (7 ms vs. 497 ms) compared to α4β2 nAChRs (**F**, **G**). Onset times for α7 and α4β2 responses showed no significant difference (**E, H**). These findings highlight distinct temporal dynamics and pharmacological sensitivities of α7 and α4β2 receptors, with α4β2 contributing to early currents overlapping with α7.

3.2 Analyses of the Difference in Tightness of Coupling Between Ca^{2+} Source and Ca^{2+} Sensor Using EGTA-AM and BAPTA-AM

In this series of experiments, the primary aim was to investigate the coupling strength between the Ca^{2+} sensor and the Ca^{2+} influx from the presynaptic voltage-gated Ca^{2+} channel (Ca^{2+} source). We employed two distinct calcium chelators, EGTA (ethylene glycol-bis(β-aminoethyl ether)-N,N,N′,N′-tetraacetic acid)-AM and BAPTA (1,2-Bis(2-aminophenoxy)ethane-N,N,N',N'-tetraacetic acid)-AM, each possessing unique dissociation constants and kinetic properties. BAPTA-AM has a faster on, binding rate (500 $\mu M^{-1}\ s^{-1}$) compared to that of EGTA-AM (9.6 $\mu M^{-1}\ s^{-1}$) (Bortolozzi, Lelli and Mammano 2008), which has the slower kinetics, making EGTA-AM particularly suited for exploring differences in the dynamics of calcium-mediated neurotransmitter release signaling within the presynaptic terminal.

3.2.1 Effect of EGTA-AM on α7 and α4β2 Nicotinic Receptor Currents

For this set of experiments recordings were again obtained from 6 cells from 6 slices from 6 mice. Following the same 20 min baseline with pharmacological inhibitors of AMPA, NMDA and $GABA_A$ receptors, EGTA-AM was applied for an additional 20 min. I observed notable effects with EGTA-AM; α4β2 area decreased by 35.5 ± 7.9% ($t(5) = 2.02$ $p = 0.022$, $n = 6$, one-tailed) (**Fig. 3-2E, Fig. 3-3A**).

Isolation of α7 responses for analysis was achieved by coapplying DHβE (10 μM) in the aCSF. The purpose of combining DHβE with EGTA in this experiment was to investigate the specific effects of EGTA on α7 responses, given our previous findings with these agents. In initial experiments, DHβE application reduced not only α4β2-mediated responses but also appeared to decrease the early peak amplitude, which we identified as a composite of both α7 and α4β2 activities around the 5–10 ms time frame. Furthermore, when EGTA was applied alone, it unexpectedly reduced the α7 peak along with α4β2 responses, which raised questions about whether this effect was due to EGTA's influence on the fast component of α4β2 that aligns temporally with α7 responses. To clarify this, we designed a follow-up experiment specifically to isolate α7 responses by coapplying DHβE with EGTA. Upon EGTA application the α7 peak current response showed no significant change ($t(4) = 0.69$, $p = 0.72$) (**Fig. 3-2C, Fig. 3-4A**). The stability of α7-mediated responses despite EGTA-AM application indicates a strong coupling of the the Ca^{2+} channels to sensor in the presynaptic boutons confering ACh mediated α7 responses; however, the presynaptic terminals of α4β2 receptors demonstrated loose coupling, leading to a 35 ± 8% reduction in the area of α4β2 following EGTA-AM application. This can be explained by EGTA's slow forward binding rate to Ca^{2+}.

3.2.2 Effect of BAPTA-AM on α7 and α4β2 nicotinic receptor responses

In this group, recordings were obtained from 5 cells from 5 mice. After a 20 min baseline recording with APV, CNQX, and gabazine to isolate nicotinic responses, BAPTA-AM (30μM) was administered for an additional 10 min alongside the pharmacological blockers. The results demonstrated a dramatic decrease in synchronous evoked nicotinic responses (**Fig. 3-2B**). α7 peak currents decreased by 71 ± 7% ($t(4) = 4.13$, $p = 0.013$, $n = 5$) (**Fig. 3-2C, Fig. 3-4B**), and the area under the curve (charge) of α4β2 nicotinic responses decreased by 71 ±

8% (t(4) = 2.131 , p = 0.0002, n = 5) (**Fig. 3-2E, Fig. 3-3B**). These findings indicate that BAPTA, due to its rapid calcium-binding capabilities, significantly disrupts the coupling between Ca^{2+} influx and neurotransmitter release, thereby affecting synchronous evoked responses of both loosely coupled and tightly coupled cholinergic synapses, which are mediating α4β2 and α7 nicotinic responses, respectively.

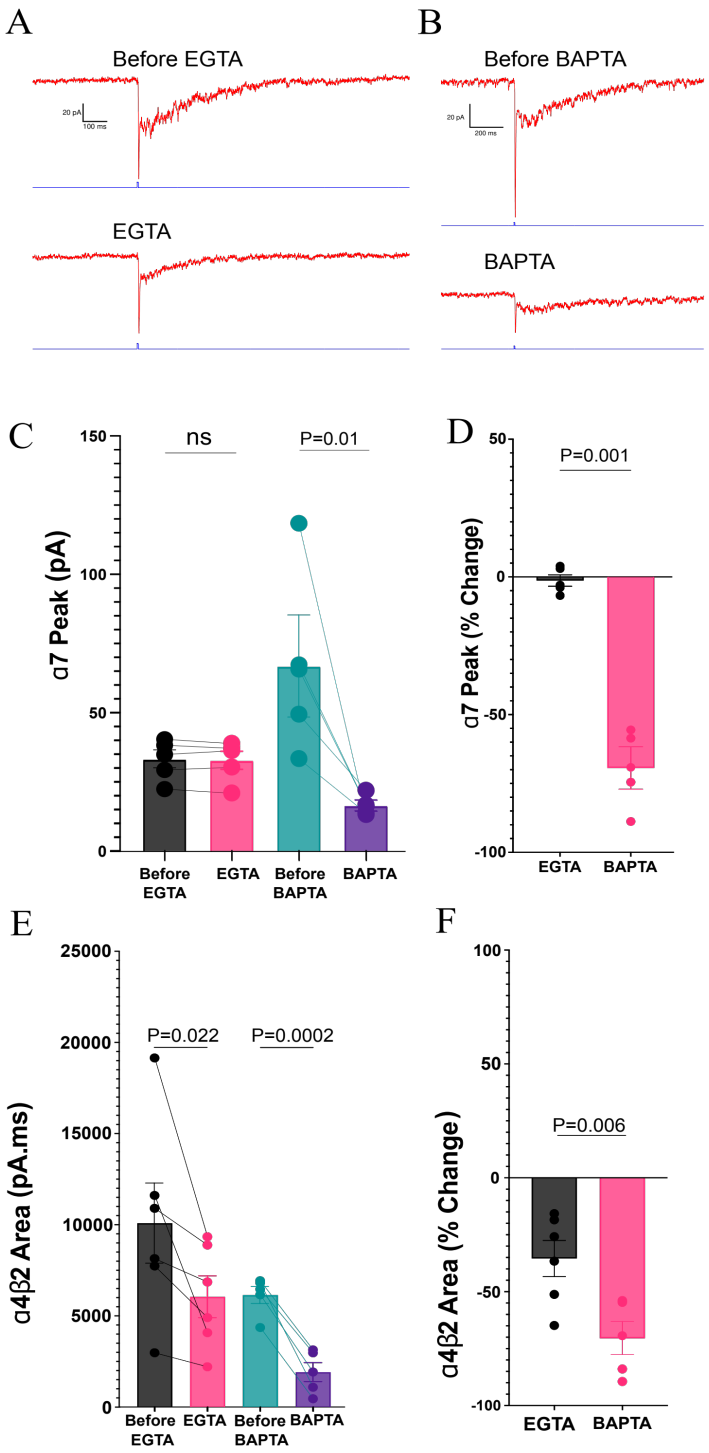

Figure 3-2 Differential effects of EGTA-AM and BAPTA-AM on α7 peak currents and α4β2 area (charge).

EGTA-AM (100 µM) caused a significant 35% decrease in the α4β2 area (**A**, **E**), while the α7 peak showed no notable changes (**C**). Note that to isolate α7 responses for analysis, DHβE (10 µM) was included in the aCSF. In

contrast, BAPTA-AM (30 µM) resulted in a dramatic 71% reduction in the α4β2 area (**B**, **F**) and a 71% decrease in the α7 peak (**D**). These findings highlight the different sensitivities of α4β2 and α7 responses to calcium chelation, with α4β2 area being markedly reduced by both chelators EGTA-AM and BAPTA-AM, while α7 peak remained unaffected by EGTA-AM.

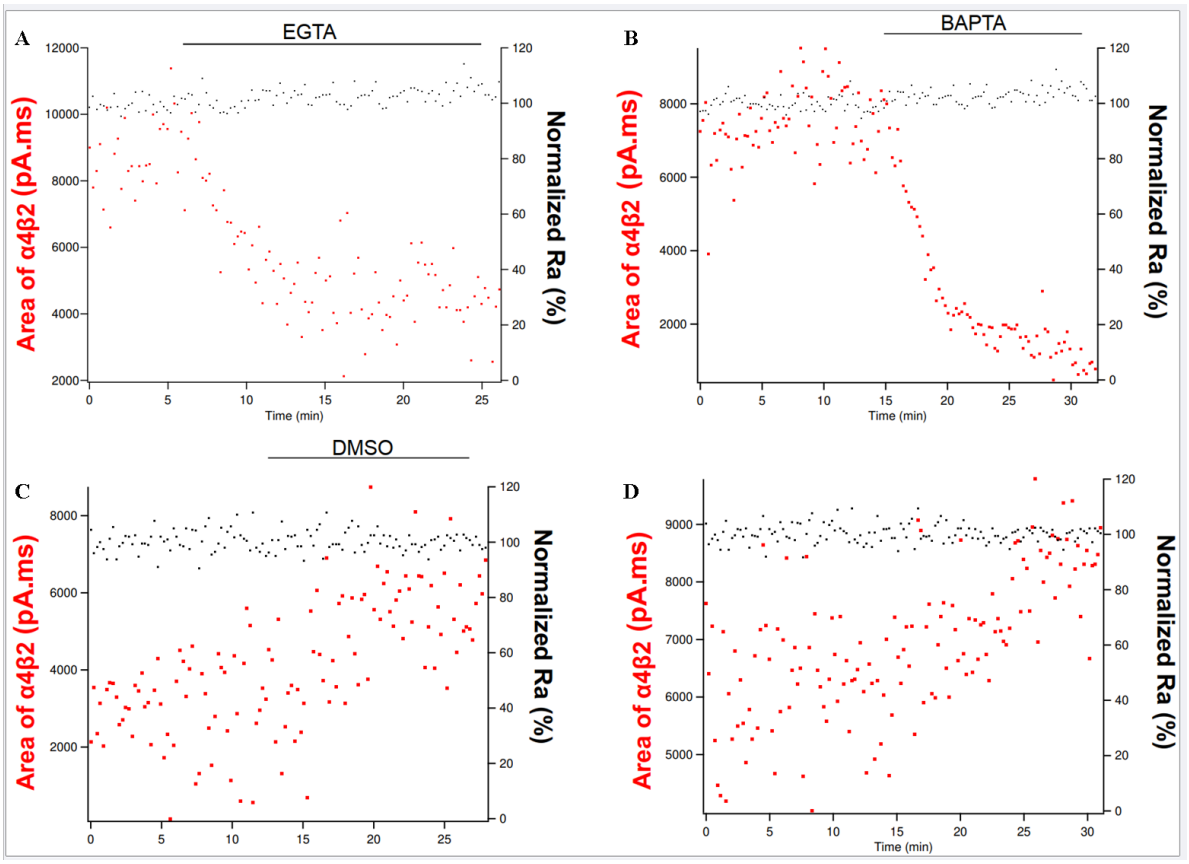

Figure 3-3 Time dependent effects of the Ca2+ chelators EGTA and BAPTA on α4β2 and α7 responses. Time dependent decrease in the area under the curve for α4β2 responses for each sweep (red circles) while 100 µM EGTA-AM was bath applied (**A**), during which the access resistance was continually monitored (black circles). BAPTA-AM (30 µM) resulted in a greater decrease in the α4β2 responses than EGTA-AM (**B**). In DMSO (0.06%) (**C**) and aCSF control experiments (**D**) the area of α4β2 increases over time, while access resistance remains unchanged. This experiment was designed to determine whether the observed reduction in α4β2 area is attributable to pharmacological effects or potential declines in cell quality over time. A 5 mV hyperpolarizing pre-pulse step was applied during the experiment with each sweep, and access resistance was calculated based on the peak current. The graph displays the area under the curve (left Y-axis, denoted in red) and normalized access resistance (right Y-axis in black). Access resistance remains stable without significant fluctuations, indicating maintained cell quality. However, the area under the curve decreases in the presence of calcium chelators, confirming that the reduction is pharmacologically driven. In DMSO and aCSF control experiments, the area increases over time while access resistance remains unchanged.

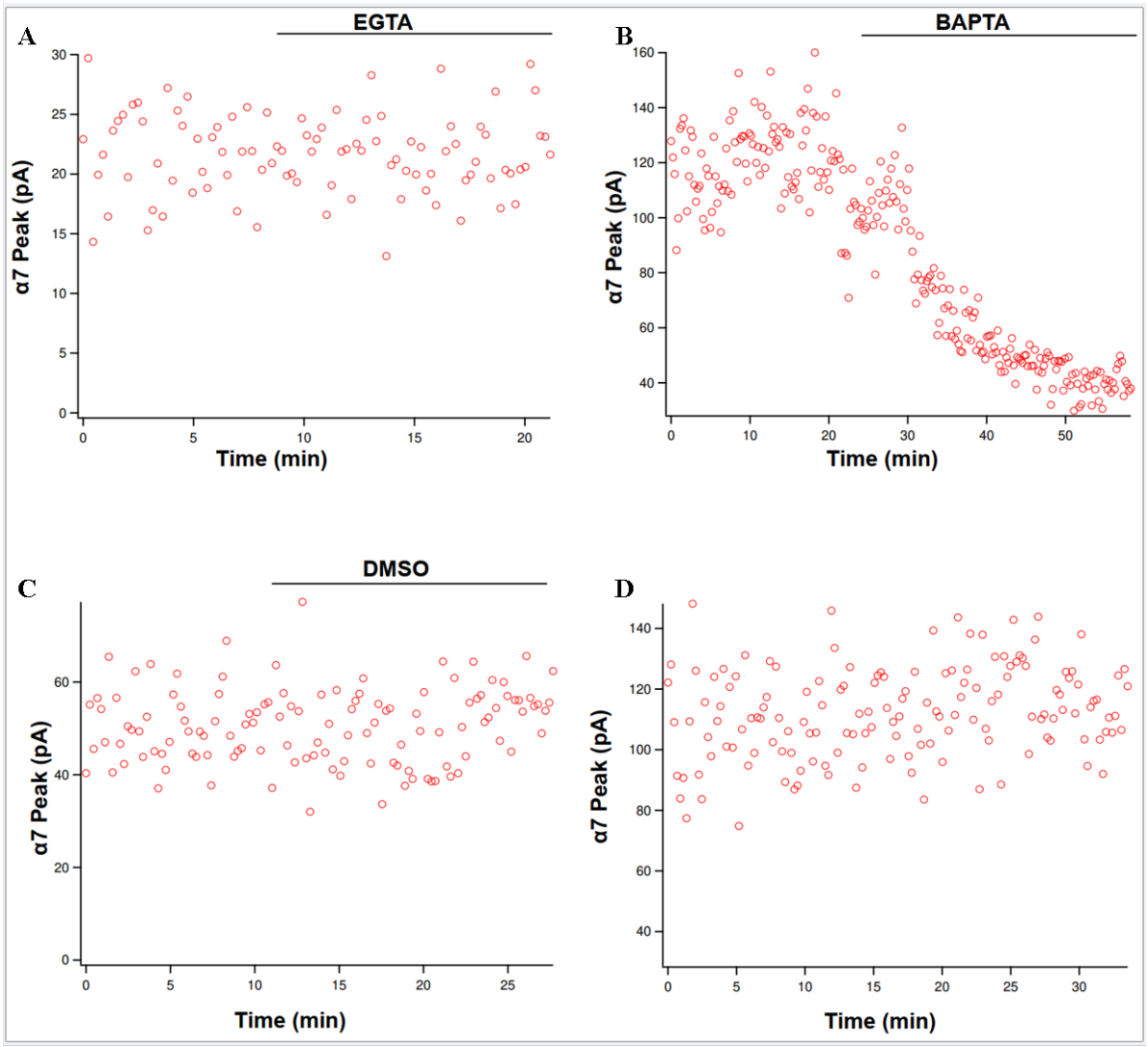

Figure 3-4 Effect of EGTA-AM and BAPTA-AM on α7 nAChR responses in layer 1 neurons of the medial prefrontal cortex.

The peak α7 currents were recorded from 5 cells across 5 mice. To isolate α7 responses, α4β2 activity was inhibited using DHβE. EGTA-AM application resulted in only a 1% change in the α7 peak (**A,** in the presence of 10 μM DHβE), suggesting a negligible effect and indicating tight coupling between the calcium source and calcium sensor for α7 nAChRs. In contrast, BAPTA-AM caused a dramatic decrease in the α7 peak, highlighting the differential sensitivity of α7 to fast calcium chelators (**B**). DMSO (0.1%) controls (5 cells) (**C**) and aCSF controls (4 cells) (**D**) exhibited no significant change in α7 peaks.

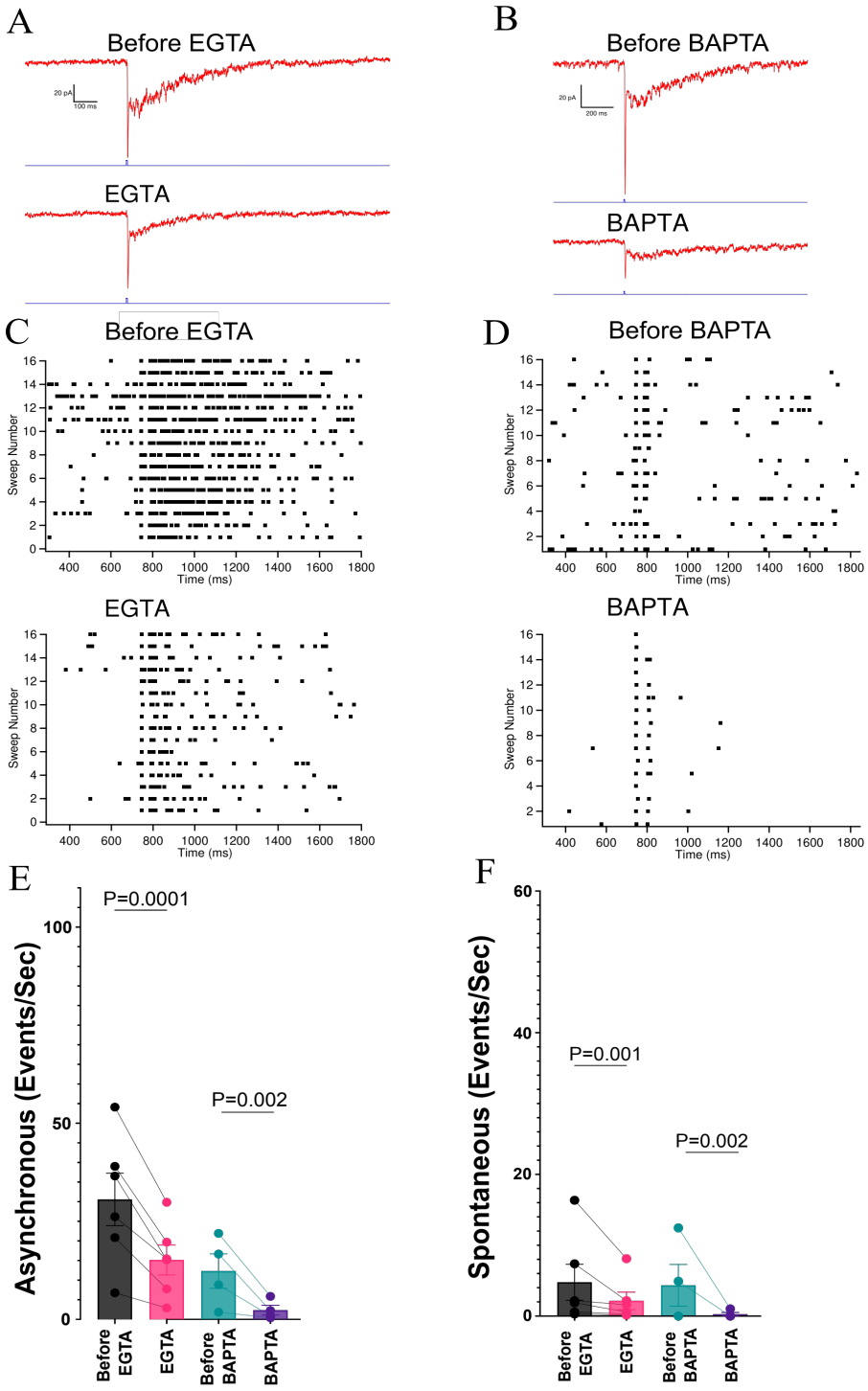

Figure 3-5 Effects of BAPTA-AM and EGTA-AM on Spontaneous and Asynchronous Events.
This figure illustrates the impact of calcium chelators BAPTA-AM and EGTA-AM on the frequency of spontaneous and asynchronous events(**A-D**). Events during the control experiment with DMSO (used to dissolve both BAPTA and EGTA) are also depicted for comparison. In the DMSO control, asynchronous events increased, while both spontaneous and asynchronous events significantly decreased after applying BAPTA-AM and EGTA-AM (**E, F**). Notably, BAPTA-AM, with its higher on-rate and dissociation constant compared to EGTA-AM, caused a greater reduction in both event types. Additionally, BAPTA-AM reduced both the peak amplitude and area of responses, whereas EGTA-AM decreased the area without affecting the peak amplitude. Event frequencies are represented as the average number of events per sweep per second.

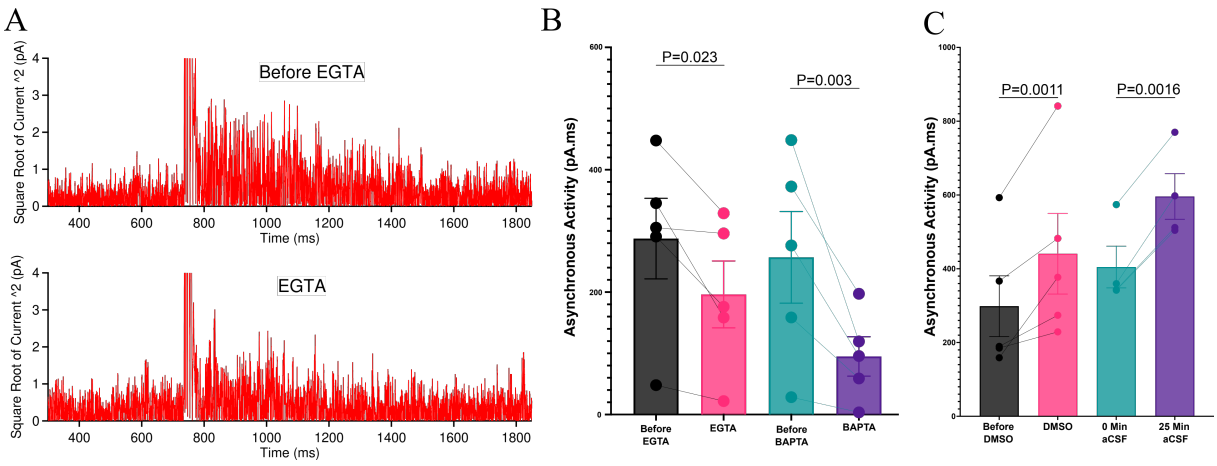

Figure 3-6 Effects of EGTA, BAPTA, and DMSO on Square Root-Transformed Area of α4β2 Responses. Comparison of square root-transformed area values for α4β2 receptor responses under baseline and treatment conditions demonstrates distinct effects of EGTA, BAPTA, and DMSO (**A**). EGTA and BAPTA treatments significantly reduced the square root area, with changes observed in six (EGTA) and five (BAPTA) experiments (**B**). In contrast, DMSO treatment resulted in a significant increase in the square root area, based on five experiments (**C**). The square root area represents the normalized charge for α4β2 responses. These findings are consistent with previous analyses of area and event detection, further confirming the effects of EGTA in diminishing α4β2 receptor activity.

3.2.3 Effect of EGTA-AM and BAPTA-AM on Spontaneous and Asynchronous Nicotinic Receptor Currents

To analyze the activity of spontaneous and asynchronous events we employed two different analyses techniques to quantify the excitatory postsynaptic events. One technique involved thresholding the events that exceeded a level that was set at twice the prestimulus baseline noise level measured from the standard deviation of the signal. Using this technique, we can count and calculate the rate of synaptic events over time (**Fig. 3-5**). We found that EGTA-AM resulted in a significant reduction of both the asynchronous ($t(5) = 9.77$, $p < 0.0001$) and spontaneous events ($t(5) = 0.57$, $p = 0.001$) (**Fig. 3-5A,C,E**). There was an even greater attenuation of asynchronous ($t(4) = 8.16$, $p = 0.002$) and spontaneous events ($t(4) = 8.16$, $p = 0.002$) with BAPTA-AM (**Fig. 3-5B,D,E**).

The second analysis methodology to study the overall activity of the events involved a technique in which we filtered out the slow kinetics of the persistent α4β2 current (band pass filter of 100 Hz high pass and a 31-point smoothing function for the low pass). Then I took the square root of the squared filtered signal to isolate the rapid transient events (**Fig. 3-6A**). Then the area was taken 20 ms post-stimulation to near the end of the trace (1100 ms later). I compared the square root-transformed area values between baseline and treatment conditions for α4β2 receptor responses, highlighting the effects of EGTA, BAPTA, and DMSO negative control. The significant decline in square root area with EGTA as compared to before EGTA (EGTA vs. Before EGTA: $t(5) = 2.614$, $p = 0.023$, $n = 6$, one-tailed) aligns with previous area-based and event detection analyses, demonstrating that EGTA reduces the asynchronous activity of α4β2 (**Fig. 3-6B**). Similarly, there was a significant decrease in in square root transformed area during BAPTA application (BAPTA vs. Before BAPTA: ($t(4) = 5.09$, $p = 0.0035$, $n = 5$)) (**Fig. 3-6B**). In contrast, the DMSO vehicle control experiment showed an increase in the square root transformed area, with 0.1% DMSO application

(DMSO vs. Before DMSO: (t(4) = 3.623, p = 0.0011, n = 5) (**Fig. 3-6C**). This increase was not a DMSO effect since a non-DMSO aCSF control showed a time dependent increase in asynchronous activity over 25 min of recording in aCSF (t(3) = 11.086, p = 0.0016, n = 4) (**Fig. 3-6C**). These results underscore the consistent impact of EGTA on diminishing asynchronous activity, confirmed across multiple analysis methods.

3.2.4 Examine Whether α7 and α4β2 Receptors Contribute to Spontaneous and Asynchronous Activity

We measured spontaneous and asynchronous activity in the presence of either MLA or DHβE to determine whether α4β2 or α7 receptors, respectively, contributes to each activity. MLA application did not have a statistically significant effect on the frequency of asynchronous events (W = 13.00, p = 0.12, n = 5) (**Fig. 3-7B, D, E**), and spontaneous events (W = 7.0, p = 0.22, n = 5) (**Fig. 3-7F**) suggesting that these events are probably mediated by α4β2 receptors rather than α7.

Upon DHβE application, a significant reduction in the area under the curve was observed, effectively eliminating the α4β2-mediated response (**Fig. 3-7A, C**), (W=-15, p-value= 0.031, n=5) (Wilcoxon Matched-Pairs Signed Rank Test). This decrease in synaptic charge corresponded with the inhibition of α4β2 receptors, which lowered asynchronous event frequency (t(4) = 7.43, p = 0.0017, n = 5) (**Fig. 3-7E**) but did not affect spontaneous activity (W = 7.0, p = 0.22, n = 5) (**Fig. 3-7F**). These results support the hypothesis that α4β2 nAChRs play a predominant role in governing asynchronous acetylcholine release, while spontaneous events remain unaffected by either α4β2 or α7 receptor inhibition (**Fig. 3-7F**). Additionally, our findings align with the proposed role of α4β2 nAChRs in modulating synaptic responses by regulating the frequency and timing of asynchronous release.

Interestingly, the peak amplitude, previously thought to reflect primarily α7 receptor activity, also showed a reduction following DHβE treatment. This suggests that α4β2 receptors have an onset that is just as fast as α7 and therefore α4β2 receptors contributes partially to the early component, which is majorly comprised of α7 current (**Fig. 3-7A**).

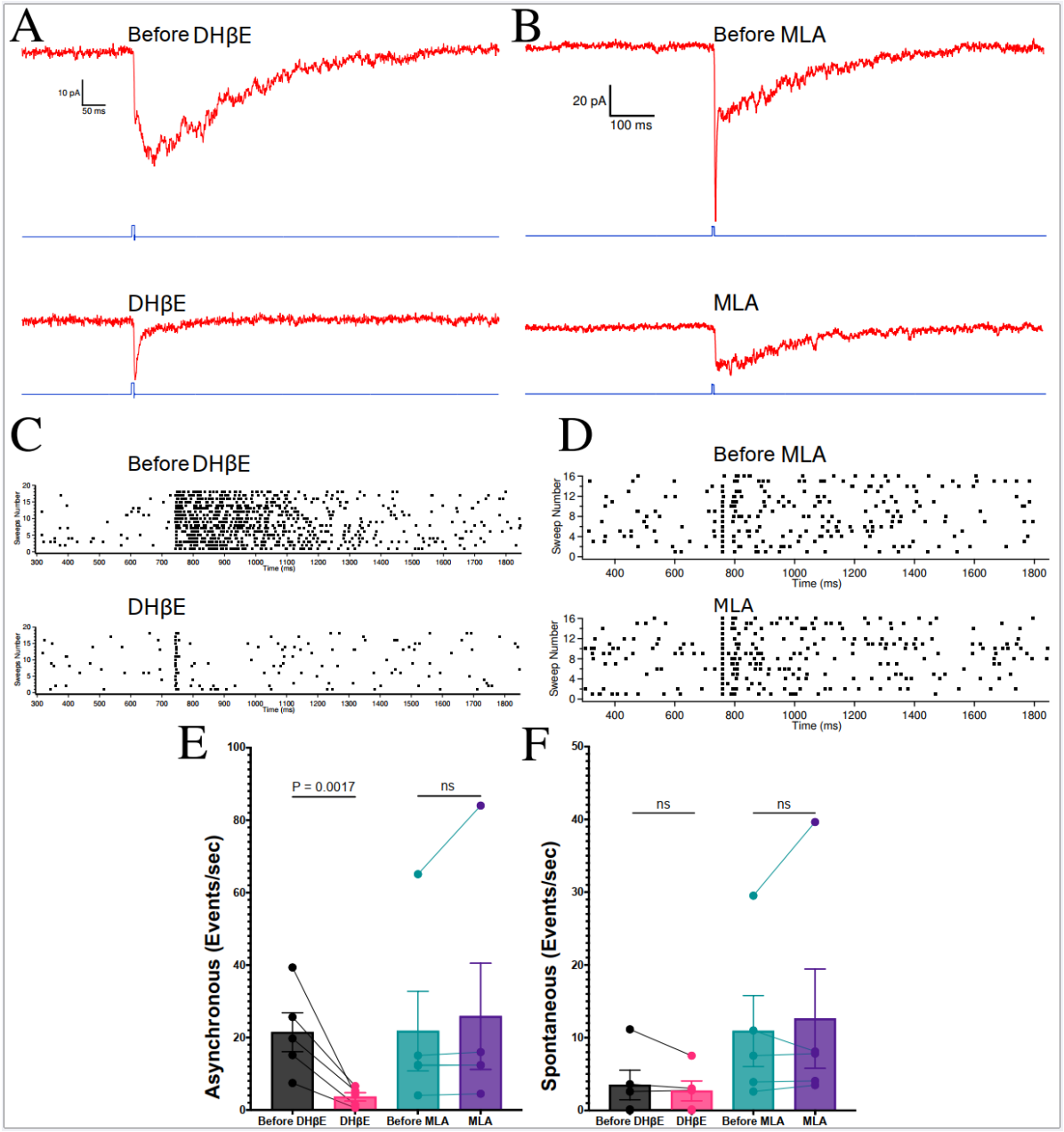

Figure 3-7 Differential effects of MLA and DHβE on asynchronous and spontaneous events in layer 1 interneurons.

Panels illustrate neuronal activity during baseline and after applying MLA (10 nM) or DHβE (10 μM) **(A, B)**. MLA did not significantly affect asynchronous or spontaneous events **(D, E, F)**, indicating that α7 nAChRs do not mediate these responses. In contrast, DHβE significantly reduced asynchronous events **(C, E)**, highlighting the predominant role of α4β2 nAChRs in mediating these responses. The area under the curve, contributed by asynchronous events, was effectively eliminated alongside α4β2 responses following the DHβE application, further supporting this conclusion. Spontaneous event frequency remained unaffected by either MLA or DHβE **(E, F)**, emphasizing distinct regulatory mechanisms for asynchronous and spontaneous release. These findings demonstrate the critical role of α4β2 nAChRs in asynchronous release and the minimal involvement of α7 nAChRs in regulating these processes.

3.3 DMSO Vehicle Control Experiments

EGTA-AM and BAPTA-AM have low solubility in water and therefore were dissolved in DMSO before diluting in aCSF. The final concentration of DMSO was 0.06% for EGTA-AM and 0.1% for BAPTA-AM. This is likely to have no physiological effect. To confirm that the low concentration of DMSO used in our experiments did not influence the observed responses, we conducted additional control experiments (in the next results section)—designated as the aCSF non-DMSO control group to examine the time dependent effect of any changes in the nicotinic responses. These control experiments allowed us to separate any potential nonspecific effects caused by the DMSO vehicle from those induced by pharmacological treatments or any time-dependent effects, independent of DMSO or pharmacology. The DMSO set of control experiments involved 5 cells from 5 brain slices from 5 different mice, which were treated with the pharmacological cocktail (APV, CNQX, and gabazine) and DMSO.

Results from the DMSO control experiments revealed a 21 ± 3% increase in α4β2 area (charge) ($t(4) = 10.751$, $p = 0.0002$, $n = 5$) (**Fig. 3-8D**) and no significant changes in asynchronous events ($t(4) = 2.051$, $p = 0.0548$, $n = 5$) (**Fig. 3-8G**) throughout the recording period, with no significant effect on α7 peak amplitude ($t(4) = 0.023$, $p = 0.49$) (**Fig. 3-8C**) or spontaneous events (**Fig. 3-8H**) upon administration of 0.1% DMSO. Unlike the results of EGTA-AM or BAPTA-AM, there was no decrease in α4β2 current area, α7 peak current, asynchronous activity or spontaneous activity. Though there was an increase in a few of these parameters, which we suspect may be due to a time-dependent effect and not a DMSO effect.

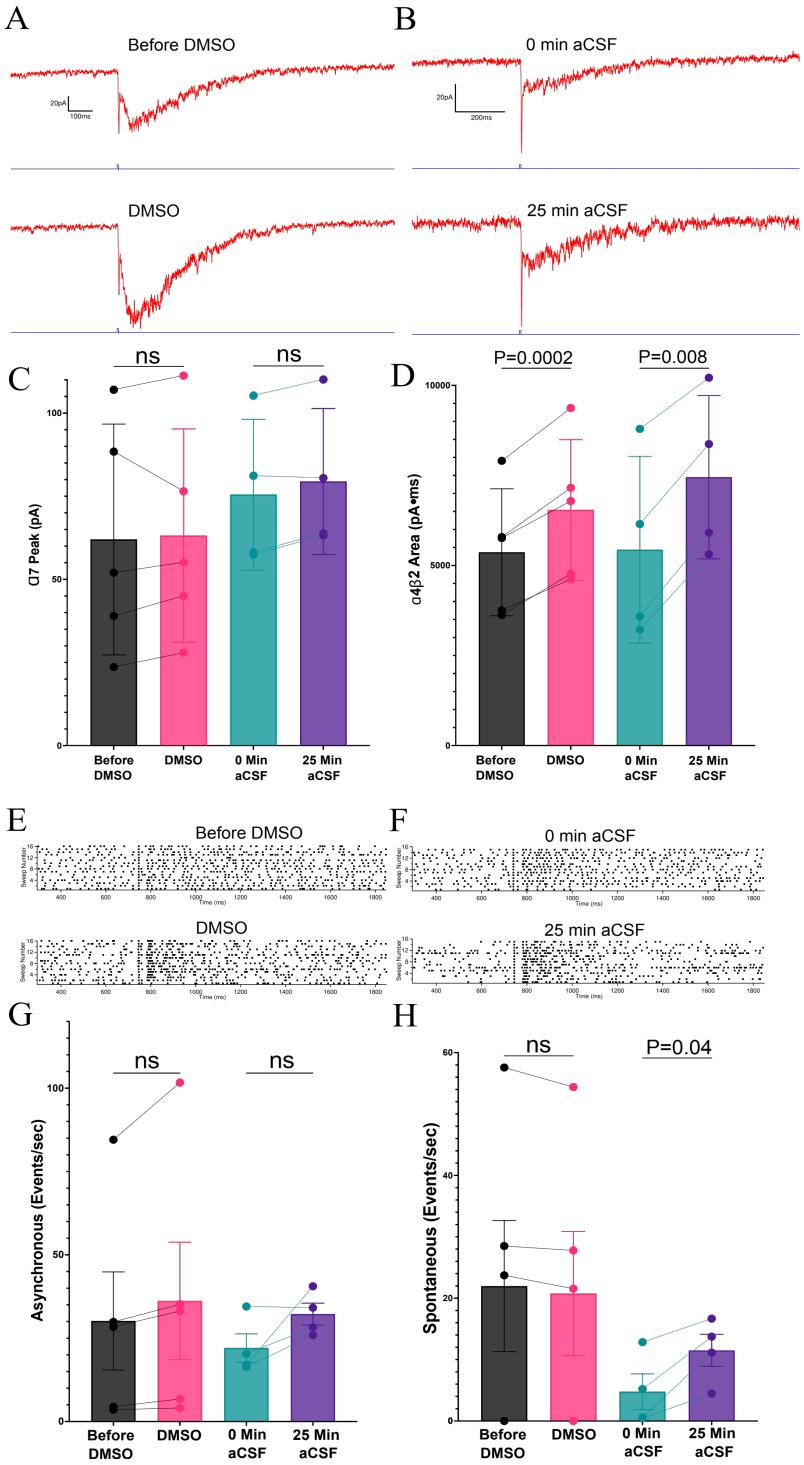

Figure 3-8 Comparison of DMSO and aCSF non-DMSO control experiments on α4β2 charge, α7 peak amplitude, asynchronous events, and spontaneous events in layer 1 interneurons.
Both DMSO (0.1%) and non-DMSO controls showed an increase in α4β2 charge over time (**A, C**, **D**), indicating that DMSO's observed effects were time-dependent rather than DMSO induced. While DMSO experiments showed a significant 21 ± 3% increase in α4β2 charge (**D**), the non-DMSO group, with fewer cells (n = 4), exhibited a similar 23 ± 3% increase in α4β2 charge. The α7 peak amplitude changes was not significant (**C**). (**E, F, G**) There was no change in asynchronous activity with either DMSO or non-DMSO aCSF controls. (**E, F H**) For spontaneous activity DMSO did not have an effect though there was an increase with non-DMSO aCSF controls.

3.4 Time-Dependent Changes of Responses in Layer 1 Interneurons

To investigate the potential impact of time on baseline neuronal responses independently of DMSO, we conducted additional control experiments designated as the aCSF non-DMSO control group. This setup allowed us to determine whether observed changes over time were due to intrinsic cellular responses rather than any effect of DMSO. This control group included 4 cells from 4 brain slices from four distinct mice, each treated solely with the pharmacological cocktail (APV, CNQX, and gabazine) to block NMDA, AMPA, and GABAergic receptors, respectively, without the inclusion of DMSO. By waiting an equivalent amount of time (25 min) as in DMSO experiments, we aimed to examine the impact of time on key metrics—charge, peak amplitude, asynchronous events, and spontaneous events.

Comparative analysis between the 0 min group and the 25 min control group showed a 23 ± 3% increase in α4β2 charge ($t(3) = 4.30$, $p = 0.008$) (**Fig. 3-8D**) and nonsignificant change in asynchronous events ($t(3) = 2.27$, $p = 0.054$, $n = 4$) (**Fig. 3-8G**) and α7 peak ($t(5.5) = 0.023$, $p = 0.49$) (**Fig. 3-8C**). However, the frequency of spontaneous events statistically increased in the 25 min condition ($t(3) = 2.64$, $p = 0.039$, $n = 4$) (**Fig. 3-8H**). From the aCSF non-DMSO control experiments, we observed that the effect of time alone was an increase in the area under the curve (charge) for α4β2 responses, indicating a gradual rise in synaptic activity over the recording period. Additionally, while the increase in asynchronous events was not statistically significant, there was a slight upward trend in their frequency, suggesting a subtle time-dependent effect on asynchronous activity. In contrast, the number of spontaneous events showed a statistically significant increase over time, indicating a clear time-dependent enhancement in spontaneous activity.

These findings indicates that the DMSO concentration had no significant effect on neurotransmission since the DMSO results were essentially equivalent in the non-DMSO aCSF controls. Therefore, we conclude that the DMSO at 0.1% employed in our experimental conditions serves as a suitable vehicle with minimal influence on the observed outcomes.

3.5 Effect of Nifedipine on Synchronous, Asynchronous and Spontaneous Events

In a subsequent series of experiments, we explored the effects of nifedipine (1 μM), an L-type calcium channel blocker, on asynchronous events, α4β2-mediated charge, and α7 peak responses. Upon application of nifedipine, we found that the charge of α4β2 responses did not decrease but rather increase ($W=-15$, $p=0.031$), which was similar to the effect of DMSO negative controls ($t(4) = 10.75$, $p = 0.0002$, $n = 5$) (**Fig. 3-9E**). Nifedipine did not affect the magnitude of the ($t(4)= 1.81$, $p=0.072$) α7 peak amplitude (**Fig. 3-9F**); similarly DMSO did not affect the amplitude of α7 current ($t(4) = 0.023$, $p = 0.49$). With nifedipine there was an increase in asynchronous events ($t(4)=2.36$, $p=0.039$) (**Fig. 3-9D**). This indicated that nifedipine had no effect on the frequency of asynchronous events. Notably, a significant finding emerged concerning spontaneous events. Following nifedipine application, the frequency of spontaneous events decreased 96 ± 9% ($W=-15$, $p = 0.031$) which was not mimicked by DMSO (**Fig. 3-9C**). This substantial reduction highlights a unique role for L-type calcium channels in the regulation of spontaneous activity, which could have

implications for understanding presynaptic calcium dynamics and spontaneous neurotransmitter release mechanisms.

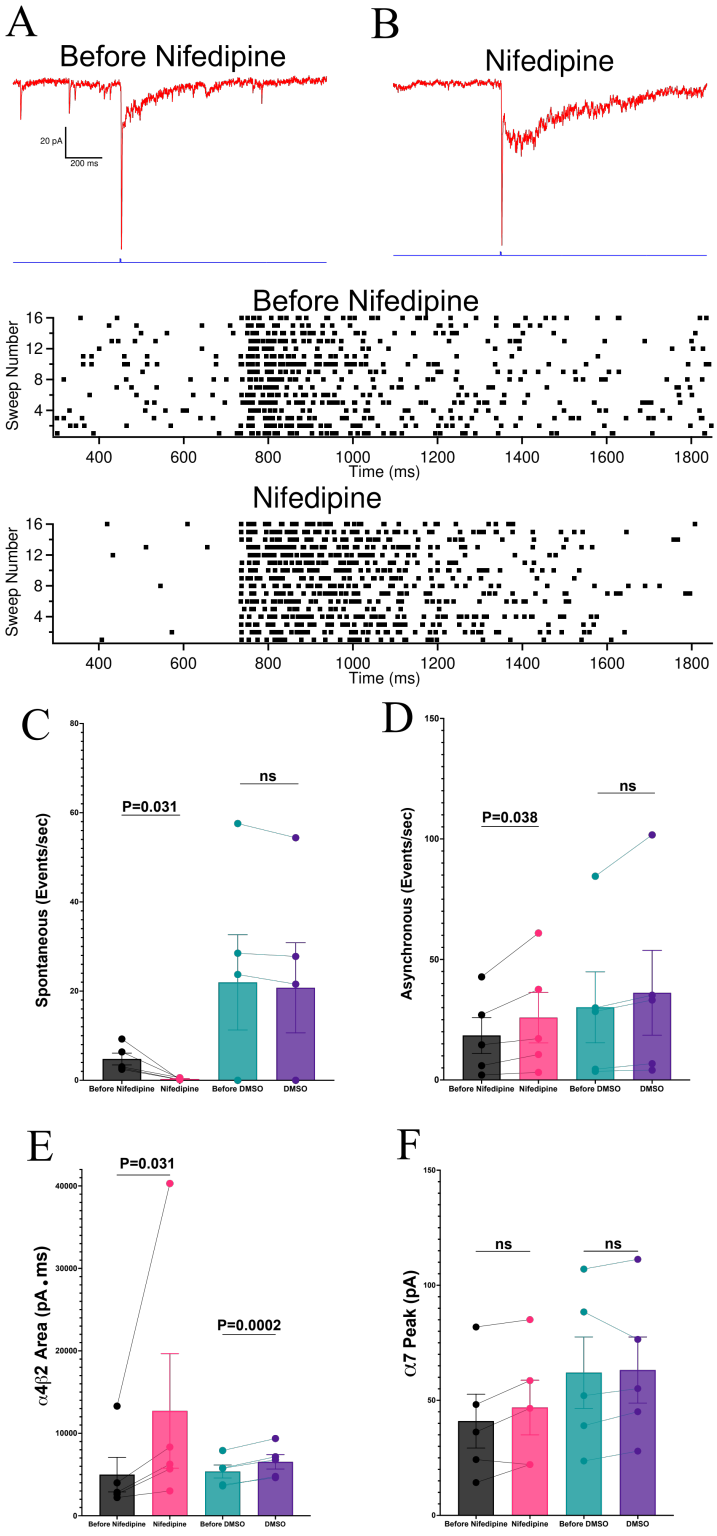

Figure 3-9 Effects of Nifedipine on α4β2-mediated charge, α7 peak amplitude, asynchronous events, and spontaneous events.

Traces of nicotinic responses before and after application of the L-type Ca^{2+} channel blocker nifedipine (1 μM) (**A, B**). Nifedipine attenuated spontaneous activity before LED stimulation unlike DMSO negative controls (**C**) but did not decrease the asynchronous activity post LED stimulation but rather increased it similar to the effect

of DMSO controls (**D**). During nifedipine application α4β2 area increased (**E**) similar to the effect of DMSO negative controls. However, nifedipine did not result in any change in the α7 peak amplitude (**F**) similar to DMSO controls.

3.6 Examining Role of Muscarinic Acetylcholine Receptors on the Slow nAChR Currents

We wanted to examine whether the slow and sustained α4β2 response could possibly be mediated by the activation of muscarinic acetylcholine receptors located either presynaptically on cholinergic terminals, whereby the muscarinic receptors could potentially couple to IP3 receptors on internal stores to drive persistent ACh release, or potentially postsynaptically. Therefore, we used atropine (500 nM) to inhibit muscarinic metabotropic receptors. Recordings were made on 5 cells from 5 brain slices from 5 different mice, maintaining the pharmacological cocktail of gabazine, CNQX and APV throughout the experiment. The introduction of atropine did not result in a diminishment of the α4β2-mediated charge but rather a significant increase in α4β2-mediated charge ($t(4) = 4.14$, $p = 0.007$, $n = 5$) (**Fig. 3-10C**) and a nonsignificant change in α7 peak amplitude ($t(4) = 0.19$, $p = 0.43$, $n = 5$) (**Fig. 3-10D**). There was no significant change in asynchronous event frequency ($t(4) = 1.90$, $p = 0.065$, $n = 5$) (**Fig. 3-10F**) nor spontaneous event frequency ($t(4) = 1.19$, $p = 0.15$, $n = 5$) (**Fig. 3-10E**) within layer 1 neurons of the prefrontal cortex. These results confirm that the observed responses are exclusively attributable to nAChR activity, with no involvement from muscarinic receptor activation.

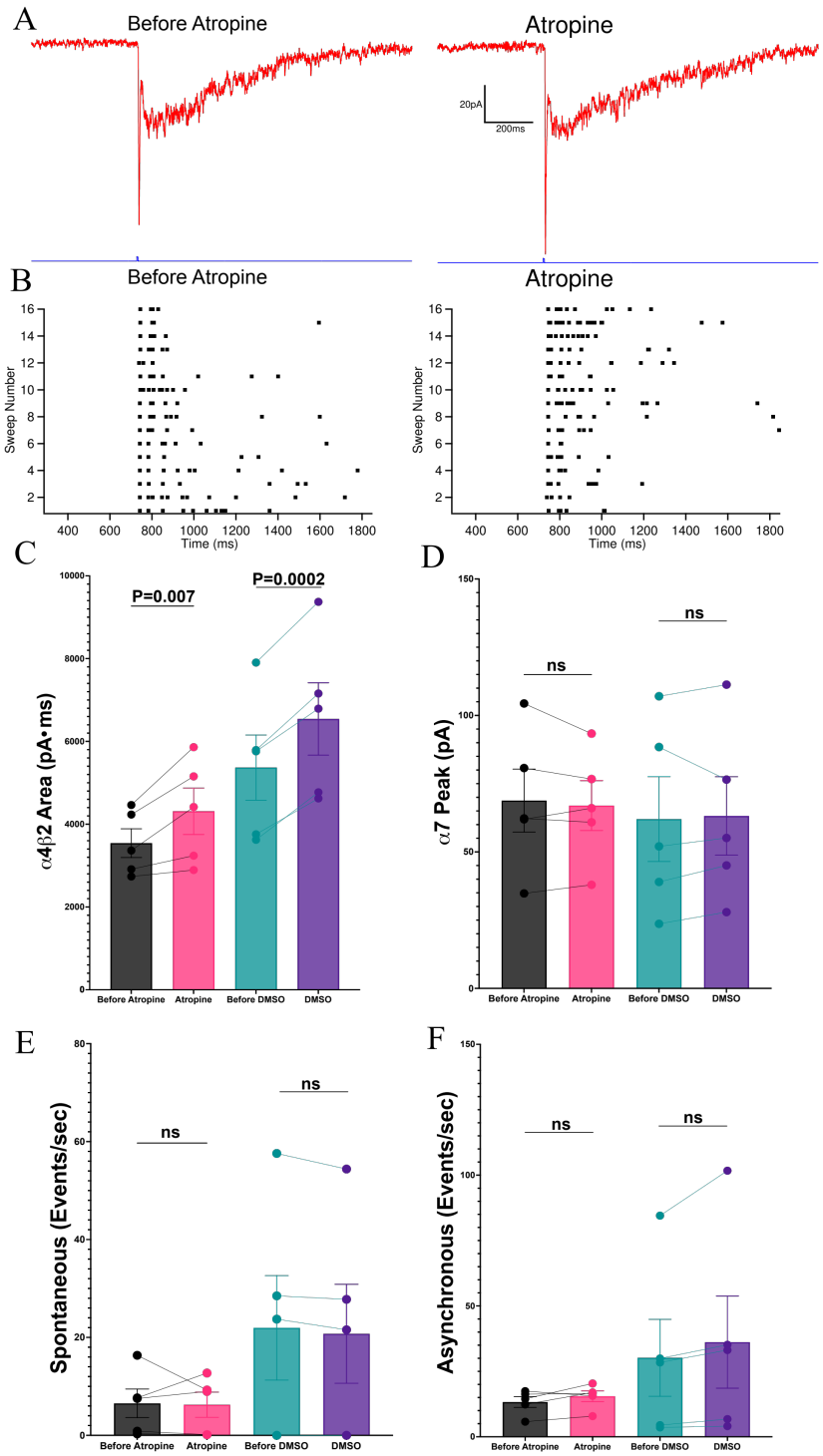

Figure 3-10 Effects of Atropine on α4β2 and α7 Responses in Layer 1 of the Prefrontal Cortex.
Traces of nicotinic responses before and after application of the muscarinic receptor inhibitor atropine (500 nM) (**A**). Raster plots showing asynchronous activity events before and during atropine application (**B**). A comparison of α4β2-mediated area (**C**), α7 peak amplitude (**D**), asynchronous event frequency (**F**), and spontaneous event frequency (**E**) before and after the application of atropine, alongside DMSO control experiments. While an increase in area was observed following atropine application, a similar increase was present in the DMSO control, indicating no specific effect of atropine on either α4β2-mediated charge or α7 peak amplitude compared to control conditions. No significant changes were noted in asynchronous or spontaneous event frequencies. Data are derived from recordings of five cells from five slices across five different mice,

confirming that the observed responses are mediated exclusively by ionotropic nicotinic acetylcholine receptors (nAChRs), without muscarinic receptor involvement.

3.7 The Effect of Altering Ca^{2+} Concentrations on Synchronous, Asynchronous and Spontaneous Activity

The objective of this experiment was to investigate the effects of varying extracellular Ca^{2+} concentrations on the activity of α4β2 and α7 receptors in layer 1 cells of the medial prefrontal cortex. Given the critical role of precise Ca^{2+} levels in modulating receptor responses, we selected Ca^{2+} concentrations based on previous studies and literature, including the work of Lanore and Silver (2016). Our earlier experiments indicated that concentrations exceeding 5 mM resulted in diminished responses (data not shown). Consequently, we chose 4 different Ca^{2+} concentrations for this experiment: 1.25 mM, 2 mM, 3 mM, and 5 mM (**Fig. 3-11A, B)**.

To ensure consistent osmolarity across all experimental conditions, we added mannitol to the aCSF to compensate for osmotic variances resulting from the varying Ca^{2+} levels. Mannitol was included as an inert osmotic agent to maintain iso-osmolarity in the aCSF solutions, preventing osmotic shifts and allowing us to isolate the effects of changes in Ca^{2+} concentration on receptor activity without inducing cellular stress.

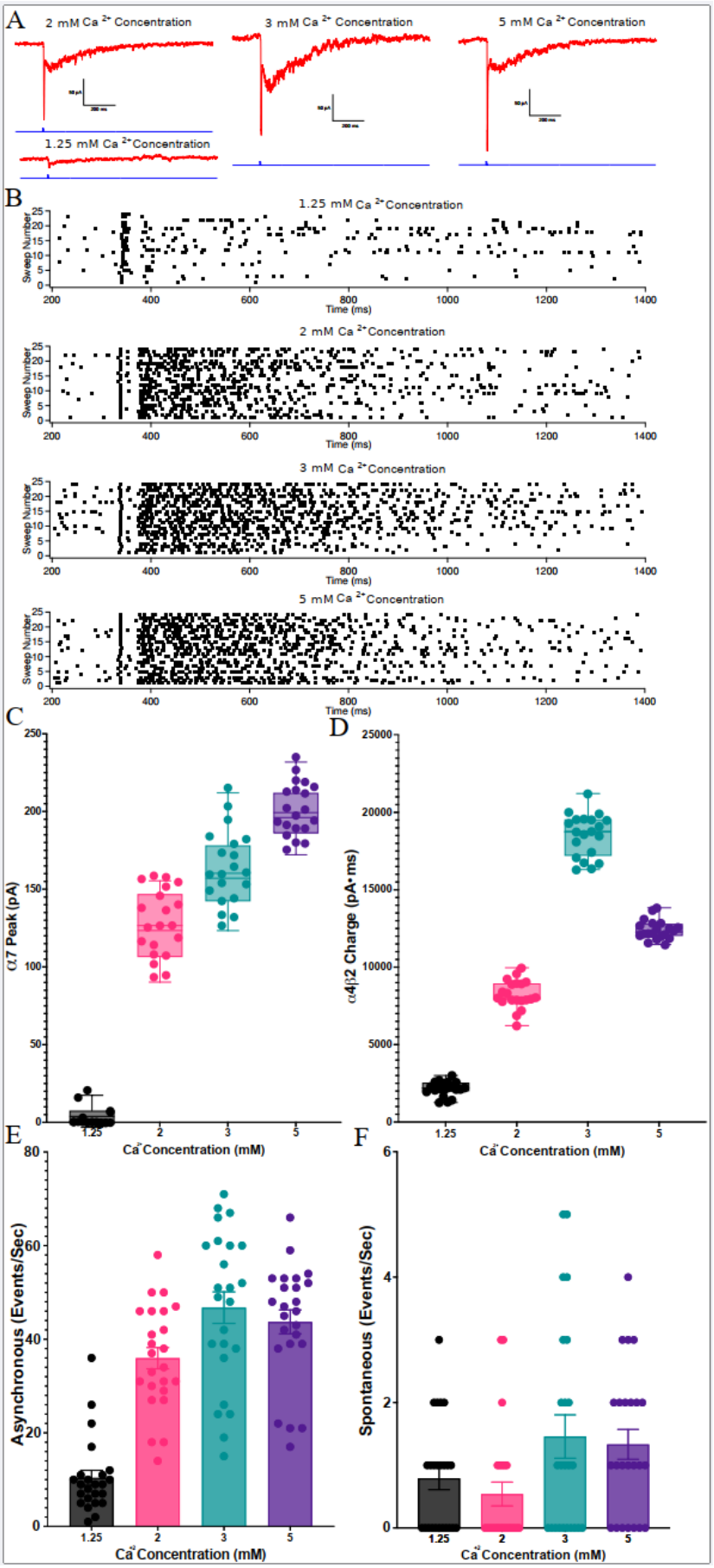
A
2 mM Ca 2+ Concentration
3 mM Ca 2+ Concentration
5 mM Ca 2+ Concentration
1.25 mM Ca 2+ Concentration
B
1.25 mM Ca 2+ Concentration
2 mM Ca 2+ Concentration
3 mM Ca 2+ Concentration
5 mM Ca 2+ Concentration
Sweep Number
Time (ms)
C
α7 Peak (pA)
D
α4β2 Charge (pA·ms)
Ca2+ Concentration (mM)
E
Asynchronous (Events/Sec)
F
Spontaneous (Events/Sec)

Figure 3-11 Effects of varying extracellular Ca^{2+} concentrations on α4β2 and α7 receptor responses in layer 1 of the medial prefrontal cortex.

This figure demonstrates the impact of increasing Ca^{2+} concentrations (1.25 mM, 2 mM, 3 mM, and 5 mM) on α4β2 and α7 receptor activity (**A, B**) on a single recorded cell. A dramatic 15.8-fold increase in α7 peak responses was observed when Ca^{2+} was increased from 1.25 mM to 2 mM, compared to a more modest 2.8-fold increase in the α4β2 area (**D**). Asynchronous event frequency also increased by 2.1-fold during this change (**E**), while spontaneous events remained unchanged (**F**). At 3 mM Ca^{2+}, a 28% increase in α7 peak amplitude and a 125% rise in α4β2 area were recorded, with corresponding increases of 30% and 112% in asynchronous and spontaneous events, respectively(**C**). However, at 5 mM Ca^{2+}, the α7 peak further increased by 23%, while the α4β2 area decreased by 33%. Asynchronous events showed a slight decline of 7%, with no changes in spontaneous events. These findings, obtained from a single experiment on one cell in one mouse, highlight the differential release probabilities and tightness of coupling mechanisms of α7 and α4β2 receptors, consistent with previous findings. . Symbols represent the measurements from multiple evoked current response traces from the same recorded cell.

Upon increasing the Ca^{2+} concentration from 1.25 mM to 2 mM, we observed a dramatic rise in α7 peak responses by 1576 ± 130% (15.76-fold) (**Fig. 3-11C)**, while the α4β2 area exhibited a more modest increase of 284 ± 26% (**Fig. 3-11D)**. Additionally, the number of asynchronous events increased by 209 ± 18% (**Fig. 3-11E**), with no change in spontaneous events (**Fig. 3-11F**). An increase to 3 mM Ca^{2+} resulted in a 28 ± 26% rise in α7 peak amplitude and a 125 ± 11% expansion of the α4β2 area (**Fig. 3-11C, D**), alongside 30 ± 3% and 112 ± 12% increases in asynchronous and spontaneous events (**Fig. 3-11E, F**), respectively. Finally, when the Ca^{2+} concentration was raised from 3 mM to 5 mM, we recorded a 23 ± 3% increase in the α7 peak current, accompanied by a 33 ± 3% reduction in the α4β2 current area (**Fig. 3-11C, D**). Asynchronous events showed a slight decline of 7 ± 1%, while spontaneous events remained unchanged.

The differential responses of the α7 and α4β2 presynaptic terminals, particularly between 1.25 mM and 2 mM Ca^{2+}, suggest different release probabilities and coupling mechanisms, with α7 exhibiting tighter coupling that mitigates EGTA's effects. These findings extend previous research and underscore the physiological differences between α7 and α4β2 release sites, confirming unique Ca^{2+} channel-to-sensor coupling and variations in release probabilities within Layer 1 cells of the medial prefrontal cortex.

Chapter 4.
Discussion & Conclusion

4.1 Overview of Findings

This study explored the activity of α4β2 and α7 nicotinic acetylcholine receptors within layer 1 of the medial prefrontal cortex. I found that cholinergic stimulation of ACh release resulted in a nAChR mediated current with two components. One of the nAChR current components was α7 mediated and characterized by MLA sensitivity and rapid current rise (2.05 ± 0.18 ms) and decay (7.4 ± 0.6 ms). The other nicotinic component was α4β2 mediated due to its sensitivity to DHβE and had a slow rise time (62.7 ± 9 ms) and slow decay time (497 ± 37 ms). α4β2 was also characterized by asynchronous activity. The ACh release mechanism mediating α7 vs α4β2 also differed. Using the Ca^{2+} chelator EGTA we found that synchronous ACh release mediating α7 responses showed a tighter coupling between Ca^{2+} source and sensor than the synchronous ACh release mediating α4β2, indicating distinct ACh release sites. The asynchronous α4β2 activity was also EGTA sensitive indicating that asynchronous activity was Ca^{2+} sensitive and showed a loose coupling between Ca^{2+} source and sensor presynaptically. Spontaneous events before light evoked activity were also inhibited by EGTA and interestingly by the L-type Ca^{2+} channel blocker nifedipine. However, nifedipine had no effect on light evoked synchronous or asynchronous activity. These spontaneous activities were not sensitive to inhibition by either DHβE nor MLA, indicating that they are ligand-gated ion channels that are not nAChR mediated, nor were they mediated by ionotropic GABAergic or glutamatergic receptors, since their respective antagonists were also present in the bath. These insights contribute to a better understanding of the specific roles of nicotinic receptors in cortical signaling, which is crucial in the research of cholinergic dysfunction in Alzheimer's disease (AD) and other neurodegenerative disorders (Rudy, Fishell et al. 2011, Kaeser and Regehr 2014).

4.2 Onsets of response of α4β2 and α7 Nicotinic Receptors

Our research findings challenge the previous understanding that fast responses were attributed solely to α7 receptors and slower, prolonged responses to α4β2 receptors as indicated in studies by Bennett et al. (2012) and Arroyo et al. (2012). Contrary to this belief, our experiments revealed that the onsets of responses for both receptor types are nearly identical. Specifically, experiments involving receptor antagonists like MLA and DHβE demonstrated that the initial fast response comprises both α7 and α4β2 currents.

We surmise as a result that postsynaptic α7 receptors are closely positioned from the presynaptic release site of ACh. However, for α4β2 receptors, based on the early component of α4β2 along with the slow build up and long persistence of the current, that α4β2 receptors occupy postsynaptic locations that are close to the presynaptic site of ACh release but are also spread further away at more distal locations from the ACh release sites. Therefore, α7 receptors signal through solely fast synaptic neurotransmission while α4β2 receptors signal through both fast synaptic transmission but also through diffuse remote volume transmission of ACh where concentrations are low at the target site. This would make sense from the stand-point of the ACh affinities of α7 vs α4β2 receptors. α7 nAChRs are homopentameric and the stoichiometry is denoted as $(\alpha7)_5$, with the subscript 5 denoting the number of subunits. α7 has very low affinity to ACh with a published EC50 of 272 μM (Briggs and McKenna 1996). This would make sense that α7 receptors are synaptic based on their low

affinity to ACh. On the other hand, α4β2 nicotinic receptors have two different stoichiometries of 5 subunits, which include $(\alpha4)_2(\beta2)_3$ and $(\alpha4)_3(\beta2)_2$ receptors. $(\alpha4)_2(\beta2)_3$ is the high affinity form of the receptor, which has an ACh EC50 of 1.1 μM, while $(\alpha4)_3(\beta2)_2$ is the low affinity receptor with an ACh EC50 of 124 μM (Zwart, Broad et al. 2006). Hence, we propose that this would allow α4β2 to subserve two functional purposes, with the high affinity form $(\alpha4)_2(\beta2)_3$ to mediate slow volume transmission distant from the release sites, while the low affinity stoichiometry $(\alpha4)_3(\beta2)_2$ to mediate fast synaptic transmission and closely situated from the ACh release sites.

Also, it should be noted that α7 and α4β2 nAChRs differ greatly in their biophysical properties regarding receptor desensitization. α7 receptors desensitizes profoundly with agonist exposure while α4β2 receptors have more modest levels of desensitization. This differential desensitization properties between α7 and α4β2 receptors would also contribute to the transient kinetics of α7 currents and the more persistent α4β2 currents.

4.3 Tightness of Coupling Between Ca Source and Ca Sensor for α4β2 vs α7 Receptors

Furthermore, we showed that α4β2 were more sensitive to EGTA than α7 responses. This suggests weaker presynaptic coupling between the Ca^{2+} source (voltage-gated Ca^{2+} channels) and sensor (synaptotagmin) for ACh containing vesicles mediating α4β2 responses than those ACh vesicles mediating α7 responses, which have a tighter coupling between Ca^{2+} source and sensor. This model suggests a presynaptic architecture, where the distance between Ca^{2+} sources (e.g. Ca^{2+} channels) and Ca^{2+} sensors (e.g. synaptotagmins) may vary depending on the receptors they modulate. For example, Ca^{2+} channels in α7 receptor containing synapses may be tightly coupled to Ca^{2+} sensors, supporting rapid, synchronous release, while those those associated with α4β2 receptors may feature looser coupling, favouring asynchronous or prolonged signaling. Such differential coupling and spatial distribution of Ca^{2+} channels could refine neurotransmitter release patterns, further integrating α4β2 into complex cholinergic signaling dynamics within the cortical circuitry.

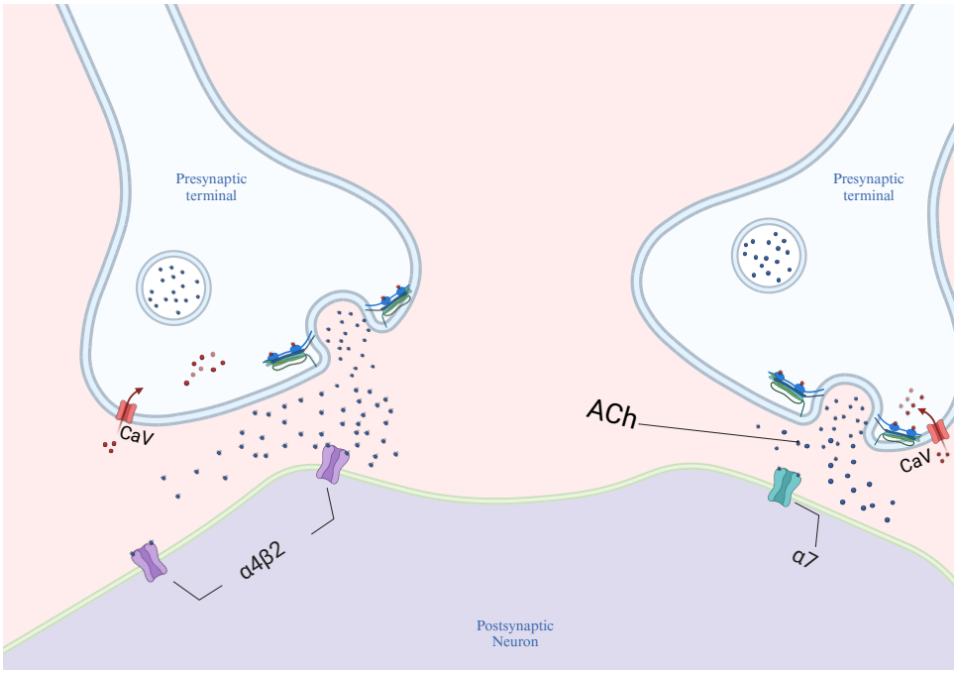

Figure 4-1 Schematic model of α4β2 and α7 Spatial Dynamics and Temporal Responses
Schematic representation illustrating the coupling tightness between Ca^{2+} channels and Ca^{2+} sensors at presynaptic terminals of α4β2 and α7 receptors. The presynaptic terminal for α4β2 exhibits loose coupling, characterized by a larger spatial distance between the Ca^{2+} source (Ca channel) and the Ca^{2+} sensor. In contrast, the α7 receptor presynaptic terminal demonstrates tight coupling, with a shorter distance between the Ca^{2+} channel and sensor. This hypothesis is supported by six experiments with EGTA, five experiments with EGTA and DHβE, and one experiment with varying Ca^{2+} concentrations, highlighting distinct coupling mechanisms for these receptor subtypes.

Schneggenburger and Rosenmund (2015) proposed that such tight coupling is characteristic of synaptic mechanisms optimized for rapid, synchronous release, commonly mediated by synaptotagmin 1 or 2, a Ca^{2+} sensor associated with fast-release events. In the case of α4β2, the loose coupling likely enables slower, asynchronous release, allowing for prolonged responses. Asynchronous neurotransmitter release has been associated with synaptotagmin 7 (Bacaj, Wu et al. 2013, Turecek and Regehr 2018). It is known that synaptotagmin 7 have 10-fold higher affinity to Ca^{2+} than either synaptotagmins 1 and 2, which have low Ca^{2+} affinities (Sugita, Shin et al. 2002). Therefore, it makes sense why synaptotagmins 1 and 2 would be immediately shut off when the presynaptic action potential repolarizes and therefore are responsible for mediating synchronous neurotransmitter release, while the high affinity synaptotagmin 7 would still be active following the action potential with the slower extrusion of residual Ca^{2+} and therefore would be capable of the delayed release of asynchronous neurotransmitter release.

This hypothesis (**Fig. 4-1**) is further supported by our Ca^{2+} concentration experiments (**Fig. 3-11**), where the response profiles of α7 and α4β2 receptors diverged as Ca^{2+} levels were varied across 1.25 mM, 2 mM, 3 mM, and 5 mM. When Ca^{2+} concentration increased from 1.25 mM to 2 mM, α7 responses showed a substantial increase, exceeding a 15-fold rise,

consistent with a high release probability typical of tightly coupled Ca^{2+} source-sensor arrangements. In contrast, α4β2 responses increased by less than four-fold, suggesting a lower release probability and a more gradual activation, aligning with its loose Ca^{2+} coupling. This differential response pattern underscores the likelihood of separate presynaptic architectures for α7 and α4β2, each with unique Ca^{2+} sensitivities and signaling roles. Kaeser et al. (2011) support this distinction, noting that synapses with tightly coupled Ca^{2+} sources respond more rapidly and robustly to changes in extracellular Ca^{2+}, whereas loosely coupled synapses are designed for prolonged neurotransmitter release.

Together, these findings suggest a model where α7 receptors are associated with presynaptic terminals optimized for rapid, synchronous release due to tight Ca^{2+} coupling, making them highly responsive to Ca^{2+}fluctuations. Conversely, α4β2 receptors appear positioned within a presynaptic environment that favours asynchronous, sustained release through looser Ca^{2+} coupling. This nuanced difference in synaptic architecture not only supports receptor-specific signaling dynamics but also offers flexibility in synaptic transmission, allowing for both immediate and extended responses based on the receptor subtype engaged. Integrating these results with earlier findings from chelator experiments reinforces the concept of distinct Ca^{2+} channel proximities and coupling efficiencies at α7 and α4β2 synaptic sites, contributing to a more comprehensive understanding of their roles in cortical processing.

4.4 Potential Role of 5-HT3 Receptors in Spontaneous Events

Despite the use of multiple receptor inhibitors (APV, CNQX, gabazine, DHβE, MLA), spontaneous events persisted, suggesting additional receptor involvement. Chartrand et al. (2023) and Rudy et al. (2011) identified the presence of 5-HT3 gene expression in layer 1 interneurons, implying that serotonergic inputs could modulate these spontaneous events. Given that 5-HT3 receptors in cortical layer 1 are primarily expressed on inhibitory interneurons, as discussed by Chartrand et al. (2023), serotonergic activity may contribute to the persistence of spontaneous responses even under Ca^{2+}-blocking conditions. Nifedipine's reduction of these events further supports the hypothesis that spontaneous serotonergic neurotransmission mediated through 5-HT3 receptors could be L-type Ca^{2+} channel-dependent. The presence of 5-HT3 receptors in the same regions as α4β2 and α7 receptors suggests a multi-receptor framework within layer 1 interneurons, which may have implications for synaptic integration and cortical modulation.

4.5 Prolonged α4β2 Response and Potential Muscarinic Involvement

We explored the possibility that the prolonged α4β2 responses, which sometimes extended up to 800 ms, was mediated by postsynaptic muscarinic receptors or presynaptic muscarinic receptor activation facilitating Ca release from internal stores through IP3 receptors in the endoplasmic reticulum. This type of IP3 signalling is known to exist for M1, M3 and M5 subtypes of muscarinic acetylcholine receptors, which are known to couple to Gαq proteins. However, atropine, a muscarinic antagonist, did not significantly impact α4β2 responses, implying that muscarinic receptors are not involved in the ACh mediated α4β2 responses both presynaptically nor postsynaptically. Future studies could explore the mechanism of Ca^{2+}

release from internal stores specifically through IP3 receptors with the selective inhibitor Xestospongin C.

4.6 Potential Mechanisms of Increased α4β2 Responses over Time

Observations in both DMSO and aCSF non-DMSO conditions revealed an increase in α4β2 response area and asynchronous frequency over time. This shows that the increase in α4β2 over time is not the effect of DMSO. The highest concentration of DMSO we used in any of the experiments to dissolve EGTA-AM was 0.06% and for BAPTA-AM was 0.1%, which is likely too low a concentration to have an effect. We do not know the underlying mechanism for the increase over time but posit two possibilities. One possibility is that a7 nAChRs are close to the soma while α4β2 are dispersed over a larger distance from the soma. With time the cesium of the pipette solution reaches further distances to block leak channels to increase the length constant of the recorded cell so that more distant synaptic input mediating α4β2 responses may be recorded. Another potential explanation is a form of long-term potentiation of α4β2 responses. However, with the infrequent stimulation frequency of once every 13.5 s makes this form of plasticity unlikely.

In the non-DMSO aCSF control experiments, the number of asynchronous events plateaued after 35 min, contrary to our initial expectation of a continued increase. This outcome may be due to a reduced sample size in this experiment, where data were recorded from 4 cells rather than the minimum of 5 cells used in other conditions. Additionally, the presence of an outlier cell, in which the asynchronous event count remained constant throughout the recording, likely contributed to this plateau. This variability impacted the overall trend, with the group narrowly failing to reach statistical significance.

4.7 Future Directions

To build on the findings in this study and clarify unresolved mechanisms, several experimental approaches could be employed, combining advanced techniques with targeted pharmacological interventions to validate and expand on observed responses in α4β2 and α7 receptors. These future studies should aim to illuminate the basis of prolonged α4β2 responses, the specific coupling of Ca^{2+} sources to synaptic release, and the receptor-specific modulation in layer 1 interneurons within the medial prefrontal cortex.

Probing the Mechanism Behind Prolonged α4β2 Responses Using IP3 and Ryanodine Receptor Blockers:

One potential cause for the prolonged response seen in α4β2 receptors is Ca^{2+} release from internal stores mediated by IP3 and ryanodine receptors. Experiments using Xestospongin C, an IP3 receptor antagonist, could help assess if these internal stores contribute to the sustained release observed in α4β2 responses. Xestospongin C has the advantage of specifically blocking IP3 receptors without inadvertently activating other pathways, unlike 2APB, which also affects TRPV1 receptors, complicating the interpretation of results. Alongside this, applying ryanodine as a selective blocker of ryanodine receptors may determine whether Ca^{2+}-induced Ca^{2+} release (CICR) mechanisms contribute to the prolonged response. If the prolonged α4β2 response decreases with either of these interventions, it would suggest that

intracellular Ca^{2+} dynamics, potentially involving both IP3 and ryanodine receptors, are key to sustaining α4β2 activation.

Calcium Imaging to Map Ca^{2+} Dynamics and Sensor-Channel Coupling at Synaptic Terminals:

Since α4β2 receptors showed sensitivity to EGTA, but α7 receptors do not, future experiments using Ca^{2+} imaging could provide a detailed analysis of the effects of EGTA on the Ca^{2+} dynamics presynaptically on cholinergic terminals and their correlation to α4β2 and α7 responses. Employing high-resolution Ca^{2+} imaging in acute brain slices with two-photon microscopy could allow the visualization of differences in Ca^{2+} concentration at α4β2 and α7 synapses, providing further understanding of Ca^{2+} source-sensor coupling. This could be paired with specific Ca^{2+} sensitive dyes or genetically encoded Ca^{2+} indicators (e.g., GCaMP) to map the duration and intensity of Ca^{2+} signals at each cholinergic synapse. Ca^{2+} imaging offers precise temporal resolution, making it ideal for visualizing the fast transient signals of α7 and the slower, prolonged responses of α4β2. Further, imaging experiments could be coupled with pharmacological tools like BAPTA or EGTA to directly assess how Ca^{2+} buffering impacts response duration, potentially clarifying if the loose Ca^{2+} coupling of α4β2 contributes to sustained activity.

Different Cholinergic Sources Contribute Differentially to Nicotinic Mediated Responses in Layer 1 Interneurons:

Layer 1 cortical neurons receive cholinergic inputs from two sources, cholinergic neurons from the basal forebrain (Bennett, Arroyo et al. 2012) and local cholinergic VIP interneurons of the cerebral cortex (Obermayer, Luchicchi et al. 2019). We would like to investigate further if there are any differences in the cholinergic neurotransmission from these two sources. Both cholinergic sources appear to mediate a rapid and transient α7 response and a slow and persistent α7. We would like to investigate whether they may differ in other aspects of their release properties including the probability of ACh release; whether they differ in their short-term synaptic plasticity of ACh release. This would require AAV cre-dependent ChR2 injection into the basal forebrain of ChATcre(neo-del) mice for the distal cholinergic projections expressing ChR2. To examine the role of VIP cholinergic interneurons we could perform dual recordings in which in addition to patching layer 1 neurons we would also target the green fluorescent neurons in the cerebral cortex of the ChATcre(neo-del)::ChR2-YFP mice.

Also, we would like to know whether these two different sources synapse to different subcellular regions along the somatodendritic extent of the layer 1 interneurons. This would require a functional mapping protocol as previously published from the Nashmi lab (Le Gratiet, Anderson et al. 2022). We would have to compare the functional cholinergic synaptic inputs between ChATcre(neo-del) mice in which AAV cre-dependent ChR2 is injected either in the basal forebrain vs the medial prefrontal cortex.

Genetic Manipulations to Investigate the Role of Synaptotagmin 7 in Asynchronous Release:

Future studies might employ genetic models, such as synaptotagmin 7 knockout mice, to examine if the persistent α4β2 responses are composed largely of asynchronous events linked to a specific Ca^{2+} sensor protein such as synaptotagmin 7. Synaptotagmin 7 has been implicated in asynchronous release (Bacaj, Wu et al. 2013), and using knockout models would allow researchers to test if asynchronous responses decrease when synaptotagmin 7 is absent. Alternatively, since synaptotagmin 1 and 2 are involved in synchronous neurotransmission (Bacaj, Wu et al. 2013), we can also use synaptotagmin 1 or 2 knockout mice to test the hypothesis that α7 responses would be abolished but α4β2 responses would remain. Additionally, knock-in mice models expressing mutant 5-HT3 receptors could help determine if serotonergic signaling contributes to the persistence of spontaneous events. Given that 5-HT3 receptors appear to influence spontaneous signaling in layer 1 interneurons (Rudy, Fishell et al. 2011), using these genetic models would clarify if serotonergic activity plays a modulatory role in cholinergic receptor dynamics, potentially pointing to broader interactions between cholinergic and serotonergic systems in the cortex.

Together, these experimental directions promise to validate and expand upon the findings presented here, shedding light on unresolved mechanisms that govern α4β2 and α7 receptor dynamics in cortical signaling.

4.8 Study Limitations

While this study provides insights into the dynamics of α4β2 and α7 nicotinic receptors in the medial prefrontal cortex, several limitations should be acknowledged. First, detecting asynchronous and spontaneous events with precision remains challenging, as these types of activity lack standardized, highly accurate detection methods. We relied on multiple analysis techniques—area under the curve, threshold-based event detection, and area of the fluctuation of current that had undergone band pass filtering and taking the square root of the square of the current—to partially mitigate this, but the intrinsic variability in such measurements could affect reproducibility. Additionally, the use of acute brain slices may limit the full observation of α4β2 and α7 responses, particularly given that slicing can result in the severing of long axonal and dendritic processes. Recording from thicker slices might address some of these structural limitations. Lastly, the prolonged recording periods could introduce artifacts related to potential run-down of currents, which could influence results, particularly in control experiments. We tried to address the current run-down issues by performing DMSO and non-DMSO aCSF controls.

Bibliography

Abbondanza, A., A. Urushadze, A. R. Alves-Barboza and H. Janickova (2024). "Expression and function of nicotinic acetylcholine receptors in specific neuronal populations: Focus on striatal and prefrontal circuits." Pharmacol Res 204: 107190.
Adesnik, H., W. Bruns, H. Taniguchi, Z. J. Huang and M. Scanziani (2012). "A neural circuit for spatial summation in visual cortex." Nature 490(7419): 226-231.
AhnAllen, C. G. (2012). "The role of the α7 nicotinic receptor in cognitive processing of persons with schizophrenia." Curr Opin Psychiatry 25(2): 103-108.
Albuquerque, E. X., E. F. Pereira, M. Alkondon and S. W. Rogers (2009). "Mammalian nicotinic acetylcholine receptors: from structure to function." Physiol Rev 89(1): 73-120.
Arroyo, S., C. Bennett, D. Aziz, S. P. Brown and S. Hestrin (2012). "Prolonged disynaptic inhibition in the cortex mediated by slow, non-α7 nicotinic excitation of a specific subset of cortical interneurons." J Neurosci 32(11): 3859-3864.
Bacaj, T., D. Wu, X. Yang, W. Morishita, P. Zhou, W. Xu, R. C. Malenka and T. C. Südhof (2013). "Synaptotagmin-1 and synaptotagmin-7 trigger synchronous and asynchronous phases of neurotransmitter release." Neuron 80(4): 947-959.
Ballinger, E. C., M. Ananth, D. A. Talmage and L. W. Role (2016). "Basal Forebrain Cholinergic Circuits and Signaling in Cognition and Cognitive Decline." Neuron 91(6): 1199-1218.
Bennett, C., S. Arroyo, D. Berns and S. Hestrin (2012). "Mechanisms generating dual-component nicotinic EPSCs in cortical interneurons." J Neurosci 32(48): 17287-17296.
Berger, T. K., G. Silberberg, R. Perin and H. Markram (2010). "Brief bursts self-inhibit and correlate the pyramidal network." PLoS Biol 8(9).
Bloem, B., L. Schoppink, D. C. Rotaru, A. Faiz, P. Hendriks, H. D. Mansvelder, W. D. van de Berg and F. G. Wouterlood (2014). "Topographic mapping between basal forebrain cholinergic neurons and the medial prefrontal cortex in mice." J Neurosci 34(49): 16234-16246.
Briggs, C. A. and D. G. McKenna (1996). "Effect of MK-801 at the human alpha 7 nicotinic acetylcholine receptor." Neuropharmacology 35(4): 407-414.
Brown, C. E., D. Sweetnam, M. Beange, P. C. Nahirney and R. Nashmi (2012). "α4* Nicotinic acetylcholine receptors modulate experience-based cortical depression in the adult mouse somatosensory cortex." J Neurosci 32(4): 1207-1219.
Changeux, J. P. (2012). "The nicotinic acetylcholine receptor: the founding father of the pentameric ligand-gated ion channel superfamily." J Biol Chem 287(48): 40207-40215.
Chartrand, T., R. Dalley, J. Close, N. A. Goriounova, B. R. Lee, R. Mann, J. A. Miller, G. Molnar, A. Mukora, L. Alfiler, K. Baker, T. E. Bakken, J. Berg, D. Bertagnolli, T. Braun, K. Brouner, T. Casper, E. A. Csajbok, N. Dee, T. Egdorf, R. Enstrom, A. A. Galakhova, A. Gary, E. Gelfand, J. Goldy, K. Hadley, T. S. Heistek, D. Hill, N. Jorstad, L. Kim, A. K. Kocsis, L. Kruse, M. Kunst, G. Leon, B. Long, M. Mallory, M. McGraw, D. McMillen, E. J. Melief, N. Mihut, L. Ng, J. Nyhus, G. Oláh, A. Ozsvár, V. Omstead, Z. Peterfi, A. Pom, L. Potekhina, R. Rajanbabu, M. Rozsa, A. Ruiz, J. Sandle, S. M. Sunkin, I. Szots, M. Tieu, M. Toth, J. Trinh, S. Vargas, D. Vumbaco, G. Williams, J. Wilson, Z. Yao, P. Barzo, C. Cobbs, R. G. Ellenbogen, L. Esposito, M. Ferreira, N. W. Gouwens, B. Grannan, R. P. Gwinn, J. S. Hauptman, T. Jarsky, C. D. Keene, A. L. Ko, C. Koch, J. G. Ojemann, A. Patel, J. Ruzevick, D. L. Silbergeld, K. Smith, S. A. Sorensen, B. Tasic, J. T. Ting, J. Waters, C. P. J. de Kock, H. D. Mansvelder, G. Tamas, H. Zeng, B. Kalmbach and E. S. Lein (2023). "Morphoelectric and transcriptomic divergence of the layer 1 interneuron repertoire in human versus mouse neocortex." Science 382(6667): eadf0805.
Chatzidaki, A. and N. S. Millar (2015). "Allosteric modulation of nicotinic acetylcholine receptors." Biochem Pharmacol 97(4): 408-417.
Chen, G. J., Z. Xiong and Z. Yan (2013). "Aβ impairs nicotinic regulation of inhibitory synaptic transmission and interneuron excitability in prefrontal cortex." Mol Neurodegener 8: 3.

Christophe, E., A. Roebuck, J. F. Staiger, D. J. Lavery, S. Charpak and E. Audinat (2002). "Two types of nicotinic receptors mediate an excitation of neocortical layer I interneurons." J Neurophysiol 88(3): 1318-1327.
Clarke, P. B., R. D. Schwartz, S. M. Paul, C. B. Pert and A. Pert (1985). "Nicotinic binding in rat brain: autoradiographic comparison of [3H]acetylcholine, [3H]nicotine, and [125I]-alpha-bungarotoxin." J Neurosci 5(5): 1307-1315.
Dajas-Bailador, F. and S. Wonnacott (2004). "Nicotinic acetylcholine receptors and the regulation of neuronal signalling." Trends Pharmacol Sci 25(6): 317-324.
Dalley, J. W., R. N. Cardinal and T. W. Robbins (2004). "Prefrontal executive and cognitive functions in rodents: neural and neurochemical substrates." Neurosci Biobehav Rev 28(7): 771-784.
Dani, J. A. and D. Bertrand (2007). "Nicotinic acetylcholine receptors and nicotinic cholinergic mechanisms of the central nervous system." Annu Rev Pharmacol Toxicol 47: 699-729.
DeFelipe, J., P. L. López-Cruz, R. Benavides-Piccione, C. Bielza, P. Larrañaga, S. Anderson, A. Burkhalter, B. Cauli, A. Fairén, D. Feldmeyer, G. Fishell, D. Fitzpatrick, T. F. Freund, G. González-Burgos, S. Hestrin, S. Hill, P. R. Hof, J. Huang, E. G. Jones, Y. Kawaguchi, Z. Kisvárday, Y. Kubota, D. A. Lewis, O. Marín, H. Markram, C. J. McBain, H. S. Meyer, H. Monyer, S. B. Nelson, K. Rockland, J. Rossier, J. L. Rubenstein, B. Rudy, M. Scanziani, G. M. Shepherd, C. C. Sherwood, J. F. Staiger, G. Tamás, A. Thomson, Y. Wang, R. Yuste and G. A. Ascoli (2013). "New insights into the classification and nomenclature of cortical GABAergic interneurons." Nat Rev Neurosci 14(3): 202-216.
Dickinson, J. A., J. N. Kew and S. Wonnacott (2008). "Presynaptic alpha 7- and beta 2-containing nicotinic acetylcholine receptors modulate excitatory amino acid release from rat prefrontal cortex nerve terminals via distinct cellular mechanisms." Mol Pharmacol 74(2): 348-359.
Drenan, R. M., S. R. Grady, A. D. Steele, S. McKinney, N. E. Patzlaff, J. M. McIntosh, M. J. Marks, J. M. Miwa and H. A. Lester (2010). "Cholinergic modulation of locomotion and striatal dopamine release is mediated by alpha6alpha4* nicotinic acetylcholine receptors." J Neurosci 30(29): 9877-9889.
Drenan, R. M., S. R. Grady, P. Whiteaker, T. McClure-Begley, S. McKinney, J. M. Miwa, S. Bupp, N. Heintz, J. M. McIntosh, M. Bencherif, M. J. Marks and H. A. Lester (2008). "In vivo activation of midbrain dopamine neurons via sensitized, high-affinity alpha 6 nicotinic acetylcholine receptors." Neuron 60(1): 123-136.
Eckenstein, F. and R. W. Baughman (1984). "Two types of cholinergic innervation in cortex, one co-localized with vasoactive intestinal polypeptide." Nature 309(5964): 153-155.
Eckenstein, F. P., R. W. Baughman and J. Quinn (1988). "An anatomical study of cholinergic innervation in rat cerebral cortex." Neuroscience 25(2): 457-474.
Eggermann, E., I. Bucurenciu, S. P. Goswami and P. Jonas (2011). "Nanodomain coupling between Ca^{2+} channels and sensors of exocytosis at fast mammalian synapses." Nat Rev Neurosci 13(1): 7-21.
Estakhr, J., D. Abazari, K. Frisby, J. M. McIntosh and R. Nashmi (2017). "Differential Control of Dopaminergic Excitability and Locomotion by Cholinergic Inputs in Mouse Substantia Nigra." Curr Biol 27(13): 1900-1914.e1904.
Fatt, P. and B. Katz (1952). "Spontaneous subthreshold activity at motor nerve endings." The Journal of physiology 117(1): 109.
Felder, C. C. (1995). "Muscarinic acetylcholine receptors: signal transduction through multiple effectors." Faseb j 9(8): 619-625.
Fredj, N. B. and J. Burrone (2009). "A resting pool of vesicles is responsible for spontaneous vesicle fusion at the synapse." Nat Neurosci 12(6): 751-758.
Fucile, S. (2004). "Ca2+ permeability of nicotinic acetylcholine receptors." Cell Calcium 35(1): 1-8.

Gamo, N. J. and A. F. Arnsten (2011). "Molecular modulation of prefrontal cortex: rational development of treatments for psychiatric disorders." Behav Neurosci 125(3): 282-296.
Gotti, C., F. Clementi, A. Fornari, A. Gaimarri, S. Guiducci, I. Manfredi, M. Moretti, P. Pedrazzi, L. Pucci and M. Zoli (2009). "Structural and functional diversity of native brain neuronal nicotinic receptors." Biochem Pharmacol 78(7): 703-711.
Gotti, C., M. Zoli and F. Clementi (2006). "Brain nicotinic acetylcholine receptors: native subtypes and their relevance." Trends Pharmacol Sci 27(9): 482-491.
Goyal, R. K. and A. Chaudhury (2013). "Structure activity relationship of synaptic and junctional neurotransmission." Auton Neurosci 176(1-2): 11-31.
Granger, A. J., W. Wang, K. Robertson, M. El-Rifai, A. F. Zanello, K. Bistrong, A. Saunders, B. W. Chow, V. Nuñez, M. Turrero García, C. C. Harwell, C. Gu and B. L. Sabatini (2020). "Cortical ChAT(+) neurons co-transmit acetylcholine and GABA in a target- and brain-region-specific manner." Elife 9.
Gritti, I., I. D. Manns, L. Mainville and B. E. Jones (2003). "Parvalbumin, calbindin, or calretinin in cortically projecting and GABAergic, cholinergic, or glutamatergic basal forebrain neurons of the rat." J Comp Neurol 458(1): 11-31.
Gubbins, E. J., M. Gopalakrishnan and J. Li (2010). "Alpha7 nAChR-mediated activation of MAP kinase pathways in PC12 cells." Brain Res 1328: 1-11.
Guillem, K., B. Bloem, R. B. Poorthuis, M. Loos, A. B. Smit, U. Maskos, S. Spijker and H. D. Mansvelder (2011). "Nicotinic acetylcholine receptor β2 subunits in the medial prefrontal cortex control attention." Science 333(6044): 888-891.
Guo, J., J. L. Ge, M. Hao, Z. C. Sun, X. S. Wu, J. B. Zhu, W. Wang, P. T. Yao, W. Lin and L. Xue (2015). "A three-pool model dissecting readily releasable pool replenishment at the calyx of held." Sci Rep 5: 9517.
Hasselmo, M. E. (2006). "The role of acetylcholine in learning and memory." Curr Opin Neurobiol 16(6): 710-715.
Heidbreder, C. A. and H. J. Groenewegen (2003). "The medial prefrontal cortex in the rat: evidence for a dorso-ventral distinction based upon functional and anatomical characteristics." Neurosci Biobehav Rev 27(6): 555-579.
Helfrich, R. F., I. C. Fiebelkorn, S. M. Szczepanski, J. J. Lin, J. Parvizi, R. T. Knight and S. Kastner (2018). "Neural Mechanisms of Sustained Attention Are Rhythmic." Neuron 99(4): 854-865.e855.
Hilscher, M. M., R. N. Leão, S. J. Edwards, K. E. Leão and K. Kullander (2017). "Chrna2-Martinotti Cells Synchronize Layer 5 Type A Pyramidal Cells via Rebound Excitation." PLoS Biol 15(2): e2001392.
Ho, T. N. T., N. Abraham and R. J. Lewis (2020). "Structure-Function of Neuronal Nicotinic Acetylcholine Receptor Inhibitors Derived From Natural Toxins." Front Neurosci 14: 609005.
Jain, A., A. Kuryatov, J. Wang, T. M. Kamenecka and J. Lindstrom (2016). "Unorthodox Acetylcholine Binding Sites Formed by α5 and β3 Accessory Subunits in α4β2* Nicotinic Acetylcholine Receptors." J Biol Chem 291(45): 23452-23463.
Jiang, M., M. Yang, L. Yin, X. Zhang and Y. Shu (2015). "Developmental reduction of asynchronous GABA release from neocortical fast-spiking neurons." Cereb Cortex 25(1): 258-270.
Kaeser, P. S. and W. G. Regehr (2014). "Molecular mechanisms for synchronous, asynchronous, and spontaneous neurotransmitter release." Annu Rev Physiol 76: 333-363.
Kaeser, P. S. and W. G. Regehr (2017). "The readily releasable pool of synaptic vesicles." Curr Opin Neurobiol 43: 63-70.
Karnani, M. M., J. Jackson, I. Ayzenshtat, A. Hamzehei Sichani, K. Manoocheri, S. Kim and R. Yuste (2016). "Opening Holes in the Blanket of Inhibition: Localized Lateral Disinhibition by VIP Interneurons." J Neurosci 36(12): 3471-3480.

Kavalali, E. T. (2015). "The mechanisms and functions of spontaneous neurotransmitter release." Nat Rev Neurosci 16(1): 5-16.
Kaeser PS, Deng L, Wang Y, Dulubova I, Liu X, Rizo J, Südhof TC. RIM proteins tether Ca2+ channels to presynaptic active zones via a direct PDZ-domain interaction. Cell. 2011 Jan 21;144(2):282-95. doi: 10.1016/j.cell.2010.12.029. PMID: 21241895; PMCID: PMC3063406.
Killcross, S. and E. Coutureau (2003). "Coordination of actions and habits in the medial prefrontal cortex of rats." Cereb Cortex 13(4): 400-408.
Kim, H., S. Ährlund-Richter, X. Wang, K. Deisseroth and M. Carlén (2016). "Prefrontal Parvalbumin Neurons in Control of Attention." Cell 164(1-2): 208-218.
Lambe, E. K., M. R. Picciotto and G. K. Aghajanian (2003). "Nicotine induces glutamate release from thalamocortical terminals in prefrontal cortex." Neuropsychopharmacology 28(2): 216-225.
Land, B. B., N. S. Narayanan, R. J. Liu, C. A. Gianessi, C. E. Brayton, D. M. Grimaldi, M. Sarhan, D. J. Guarnieri, K. Deisseroth, G. K. Aghajanian and R. J. DiLeone (2014). "Medial prefrontal D1 dopamine neurons control food intake." Nat Neurosci 17(2): 248-253.
Lanore, F. and R. A. Silver (2016). "Extracting quantal properties of transmission at central synapses." Neuromethods 113: 193-211.
Le Gratiet, K. L., C. K. Anderson, N. Puente, P. Grandes, C. Copas, P. C. Nahirney, K. R. Delaney and R. Nashmi (2022). "Differential Subcellular Distribution and Release Dynamics of Cotransmitted Cholinergic and GABAergic Synaptic Inputs Modify Dopaminergic Neuronal Excitability." J Neurosci 42(46): 8670-8693.
Lee, S., I. Kruglikov, Z. J. Huang, G. Fishell and B. Rudy (2013). "A disinhibitory circuit mediates motor integration in the somatosensory cortex." Nat Neurosci 16(11): 1662-1670.
Leung, J., D. M. McPhee, A. Renda, N. Penty, F. Farhoomand, R. Nashmi and K. R. Delaney (2017). "MeCP2-deficient mice have reduced α4 and α6 nicotinic receptor mRNA and altered behavioral response to nicotinic agonists." Behav Brain Res 330: 118-126.
Levin, E. D., A. Petro, A. H. Rezvani, N. Pollard, N. C. Christopher, M. Strauss, J. Avery, J. Nicholson and J. E. Rose (2009). "Nicotinic alpha7- or beta2-containing receptor knockout: effects on radial-arm maze learning and long-term nicotine consumption in mice." Behav Brain Res 196(2): 207-213.
Loewi, O. (1924). "Über humorale Übertragbarkeit der Herznervenwirkung: IV. Mitteilung." Pflüger's Archiv für die gesamte Physiologie des Menschen und der Tiere 204: 361-367.
Luo, F., T. Bacaj and T. C. Südhof (2015). "Synaptotagmin-7 Is Essential for Ca2+-Triggered Delayed Asynchronous Release But Not for Ca2+-Dependent Vesicle Priming in Retinal Ribbon Synapses." J Neurosci 35(31): 11024-11033.
Mansvelder, H. D., J. R. Keath and D. S. McGehee (2002). "Synaptic mechanisms underlie nicotine-induced excitability of brain reward areas." Neuron 33(6): 905-919.
Mansvelder, H. D. and D. S. McGehee (2000). "Long-term potentiation of excitatory inputs to brain reward areas by nicotine." Neuron 27(2): 349-357.
Marks, M. J., J. R. Pauly, S. D. Gross, E. S. Deneris, I. Hermans-Borgmeyer, S. F. Heinemann and A. C. Collins (1992). "Nicotine binding and nicotinic receptor subunit RNA after chronic nicotine treatment." J Neurosci 12(7): 2765-2784.
Marra, V., J. J. Burden, J. R. Thorpe, I. T. Smith, S. L. Smith, M. Häusser, T. Branco and K. Staras (2012). "A preferentially segregated recycling vesicle pool of limited size supports neurotransmission in native central synapses." Neuron 76(3): 579-589.
Matsubayashi, H., T. Amano, T. Seki, M. Sasa and N. Sakai (2004). "Postsynaptic alpha 4 beta 2 and alpha 7 type nicotinic acetylcholine receptors contribute to the local and endogenous acetylcholine-mediated synaptic transmissions in nigral dopaminergic neurons." Brain Res 1005(1-2): 1-8.

Mehta, B., J. Snellman, S. Chen, W. Li and D. Zenisek (2013). "Synaptic ribbons influence the size and frequency of miniature-like evoked postsynaptic currents." Neuron 77(3): 516-527.
Michel, K., J. A. Müller, A. M. Oprişoreanu and S. Schoch (2015). "The presynaptic active zone: A dynamic scaffold that regulates synaptic efficacy." Exp Cell Res 335(2): 157-164.
Murthy, V. N., T. Schikorski, C. F. Stevens and Y. Zhu (2001). "Inactivity produces increases in neurotransmitter release and synapse size." Neuron 32(4): 673-682.
Neher, E. and T. Sakaba (2008). "Multiple roles of calcium ions in the regulation of neurotransmitter release." Neuron 59(6): 861-872.
Nieuwenhuys, R. (1994). "The neocortex. An overview of its evolutionary development, structural organization and synaptology." Anat Embryol (Berl) 190(4): 307-337.
Obermayer, J., A. Luchicchi, T. S. Heistek, S. F. de Kloet, H. Terra, B. Bruinsma, O. Mnie-Filali, C. Kortleven, A. A. Galakhova, A. J. Khalil, T. Kroon, A. J. Jonker, R. de Haan, W. D. J. van de Berg, N. A. Goriounova, C. P. J. de Kock, T. Pattij and H. D. Mansvelder (2019). "Prefrontal cortical ChAT-VIP interneurons provide local excitation by cholinergic synaptic transmission and control attention." Nat Commun 10(1): 5280.
Obermayer, J., A. Luchicchi, T. S. Heistek, S. F. de Kloet, H. Terra, B. Bruinsma, O. Mnie-Filali, C. Kortleven, A. A. Galakhova, A. J. Khalil, T. Kroon, A. J. Jonker, R. de Haan, W. D. J. van de Berg, N. A. Goriounova, C. P. J. de Kock, T. Pattij and H. D. Mansvelder (2020). "Author Correction: Prefrontal cortical ChAT-VIP interneurons provide local excitation by cholinergic synaptic transmission and control attention." Nat Commun 11(1): 794.
Otsu, Y., V. Shahrezaei, B. Li, L. A. Raymond, K. R. Delaney and T. H. Murphy (2004). "Competition between phasic and asynchronous release for recovered synaptic vesicles at developing hippocampal autaptic synapses." J Neurosci 24(2): 420-433.
Parikh, V., R. Kozak, V. Martinez and M. Sarter (2007). "Prefrontal acetylcholine release controls cue detection on multiple timescales." Neuron 56(1): 141-154.
Patel, A. V., A. Nguyen, P. Paletta, E. Choleris and C. D. Bailey (2023). "Prefrontal layer V pyramidal neurons comprise multiple subtypes with distinct nicotinic responses and projection targets." bioRxiv: 2023.2004. 2010.536291.
Pedersen, J. E., C. A. Bergqvist and D. Larhammar (2019). "Evolution of vertebrate nicotinic acetylcholine receptors." BMC Evol Biol 19(1): 38.
Perry, E., C. Martin-Ruiz, M. Lee, M. Griffiths, M. Johnson, M. Piggott, V. Haroutunian, J. D. Buxbaum, J. Nãsland, K. Davis, C. Gotti, F. Clementi, S. Tzartos, O. Cohen, H. Soreq, E. Jaros, R. Perry, C. Ballard, I. McKeith and J. Court (2000). "Nicotinic receptor subtypes in human brain ageing, Alzheimer and Lewy body diseases." Eur J Pharmacol 393(1-3): 215-222.
Pi, H. J., B. Hangya, D. Kvitsiani, J. I. Sanders, Z. J. Huang and A. Kepecs (2013). "Cortical interneurons that specialize in disinhibitory control." Nature 503(7477): 521-524.
Picciotto, M. R., M. J. Higley and Y. S. Mineur (2012). "Acetylcholine as a neuromodulator: cholinergic signaling shapes nervous system function and behavior." Neuron 76(1): 116-129.
Poorthuis, R. B., B. Bloem, B. Schak, J. Wester, C. P. de Kock and H. D. Mansvelder (2013). "Layer-specific modulation of the prefrontal cortex by nicotinic acetylcholine receptors." Cereb Cortex 23(1): 148-161.
Pouille, F. and M. Scanziani (2001). "Enforcement of temporal fidelity in pyramidal cells by somatic feed-forward inhibition." Science 293(5532): 1159-1163.
Price, J. L. and R. Stern (1983). "Individual cells in the nucleus basalis--diagonal band complex have restricted axonal projections to the cerebral cortex in the rat." Brain Res 269(2): 352-356.
Qiu, X., Q. Zhu and J. Sun (2015). "Quantitative analysis of vesicle recycling at the calyx of Held synapse." Proc Natl Acad Sci U S A 112(15): 4779-4784.

Rey, S. A., C. A. Smith, M. W. Fowler, F. Crawford, J. J. Burden and K. Staras (2015). "Ultrastructural and functional fate of recycled vesicles in hippocampal synapses." Nat Commun 6: 8043.
Riga, D., M. R. Matos, A. Glas, A. B. Smit, S. Spijker and M. C. Van den Oever (2014). "Optogenetic dissection of medial prefrontal cortex circuitry." Front Syst Neurosci 8: 230.
Rizo, J. (2022). "Molecular Mechanisms Underlying Neurotransmitter Release." Annu Rev Biophys 51: 377-408.
Roerig, B., D. A. Nelson and L. C. Katz (1997). "Fast synaptic signaling by nicotinic acetylcholine and serotonin 5-HT3 receptors in developing visual cortex." J Neurosci 17(21): 8353-8362.
Rudy, B., G. Fishell, S. Lee and J. Hjerling-Leffler (2011). "Three groups of interneurons account for nearly 100% of neocortical GABAergic neurons." Dev Neurobiol 71(1): 45-61.
Rye, D. B., B. H. Wainer, M. M. Mesulam, E. J. Mufson and C. B. Saper (1984). "Cortical projections arising from the basal forebrain: a study of cholinergic and noncholinergic components employing combined retrograde tracing and immunohistochemical localization of choline acetyltransferase." Neuroscience 13(3): 627-643.
Sara, Y., M. G. Mozhayeva, X. Liu and E. T. Kavalali (2002). "Fast vesicle recycling supports neurotransmission during sustained stimulation at hippocampal synapses." J Neurosci 22(5): 1608-1617.
Sarter, M., V. Parikh and W. M. Howe (2009). "nAChR agonist-induced cognition enhancement: integration of cognitive and neuronal mechanisms." Biochem Pharmacol 78(7): 658-667.
Sarter, M., V. Parikh and W. M. Howe (2009). "Phasic acetylcholine release and the volume transmission hypothesis: time to move on." Nat Rev Neurosci 10(5): 383-390.
Schneggenburger, R. and C. Rosenmund (2015). "Molecular mechanisms governing Ca(2+) regulation of evoked and spontaneous release." Nat Neurosci 18(7): 935-941.
Schuman, B., S. Dellal, A. Prönneke, R. Machold and B. Rudy (2021). "Neocortical Layer 1: An Elegant Solution to Top-Down and Bottom-Up Integration." Annu Rev Neurosci 44: 221-252.
Schuman, B., R. P. Machold, Y. Hashikawa, J. Fuzik, G. J. Fishell and B. Rudy (2019). "Four Unique Interneuron Populations Reside in Neocortical Layer 1." J Neurosci 39(1): 125-139.
Silberberg, G. and H. Markram (2007). "Disynaptic inhibition between neocortical pyramidal cells mediated by Martinotti cells." Neuron 53(5): 735-746.
Sparks, D. L., T. G. Beach and R. J. Lukas (1998). "Immunohistochemical localization of nicotinic beta2 and alpha4 receptor subunits in normal human brain and individuals with Lewy body and Alzheimer's disease: preliminary observations." Neurosci Lett 256(3): 151-154.
Südhof, T. C. (1995). "The synaptic vesicle cycle: a cascade of protein-protein interactions." Nature 375(6533): 645-653.
Südhof, T. C. (2000). "The synaptic vesicle cycle revisited." Neuron 28(2): 317-320.
Sugita, S., O. H. Shin, W. Han, Y. Lao and T. C. Südhof (2002). "Synaptotagmins form a hierarchy of exocytotic Ca(2+) sensors with distinct Ca(2+) affinities." Embo j 21(3): 270-280.
Sun, Q. Q., J. R. Huguenard and D. A. Prince (2006). "Barrel cortex microcircuits: thalamocortical feedforward inhibition in spiny stellate cells is mediated by a small number of fast-spiking interneurons." J Neurosci 26(4): 1219-1230.
Sydserff, S., E. J. Sutton, D. Song, M. C. Quirk, C. Maciag, C. Li, G. Jonak, D. Gurley, J. C. Gordon, E. P. Christian, J. J. Doherty, T. Hudzik, E. Johnson, L. Mrzljak, T. Piser, G. N. Smagin, Y. Wang, D. Widzowski and J. S. Smith (2009). "Selective alpha7 nicotinic receptor activation by AZD0328 enhances cortical dopamine release and improves learning and attentional processes." Biochem Pharmacol 78(7): 880-888.
Tang, A. H., H. Chen, T. P. Li, S. R. Metzbower, H. D. MacGillavry and T. A. Blanpied (2016). "A trans-synaptic nanocolumn aligns neurotransmitter release to receptors." Nature 536(7615): 210-214.

Tasic, B., V. Menon, T. N. Nguyen, T. K. Kim, T. Jarsky, Z. Yao, B. Levi, L. T. Gray, S. A. Sorensen, T. Dolbeare, D. Bertagnolli, J. Goldy, N. Shapovalova, S. Parry, C. Lee, K. Smith, A. Bernard, L. Madisen, S. M. Sunkin, M. Hawrylycz, C. Koch and H. Zeng (2016). "Adult mouse cortical cell taxonomy revealed by single cell transcriptomics." Nat Neurosci 19(2): 335-346.
Tasic, B., Z. Yao, L. T. Graybuck, K. A. Smith, T. N. Nguyen, D. Bertagnolli, J. Goldy, E. Garren, M. N. Economo, S. Viswanathan, O. Penn, T. Bakken, V. Menon, J. Miller, O. Fong, K. E. Hirokawa, K. Lathia, C. Rimorin, M. Tieu, R. Larsen, T. Casper, E. Barkan, M. Kroll, S. Parry, N. V. Shapovalova, D. Hirschstein, J. Pendergraft, H. A. Sullivan, T. K. Kim, A. Szafer, N. Dee, P. Groblewski, I. Wickersham, A. Cetin, J. A. Harris, B. P. Levi, S. M. Sunkin, L. Madisen, T. L. Daigle, L. Looger, A. Bernard, J. Phillips, E. Lein, M. Hawrylycz, K. Svoboda, A. R. Jones, C. Koch and H. Zeng (2018). "Shared and distinct transcriptomic cell types across neocortical areas." Nature 563(7729): 72-78.
Thiele, A. and M. A. Bellgrove (2018). "Neuromodulation of Attention." Neuron 97(4): 769-785.
Thomsen, M. S., H. H. Hansen, D. B. Timmerman and J. D. Mikkelsen (2010). "Cognitive improvement by activation of alpha7 nicotinic acetylcholine receptors: from animal models to human pathophysiology." Curr Pharm Des 16(3): 323-343.
Ting JT, Daigle TL, Chen Q, Feng G (2014) Acute brain slice methods for adult and aging animals: application of targeted patch clamp analysis and optogenetics. Methods Mol Biol Clifton NJ 1183:221–242.
Tremblay, R., S. Lee and B. Rudy (2016). "GABAergic Interneurons in the Neocortex: From Cellular Properties to Circuits." Neuron 91(2): 260-292.
Turecek, J. and W. G. Regehr (2018). "Synaptotagmin 7 Mediates Both Facilitation and Asynchronous Release at Granule Cell Synapses." J Neurosci 38(13): 3240-3251.
Verhoog, M. B., J. Obermayer, C. A. Kortleven, R. Wilbers, J. Wester, J. C. Baayen, C. P. J. De Kock, R. M. Meredith and H. D. Mansvelder (2016). "Layer-specific cholinergic control of human and mouse cortical synaptic plasticity." Nat Commun 7: 12826.
von Engelhardt, J., M. Eliava, A. H. Meyer, A. Rozov and H. Monyer (2007). "Functional characterization of intrinsic cholinergic interneurons in the cortex." J Neurosci 27(21): 5633-5642.
Wang, J., A. Kuryatov, A. Sriram, Z. Jin, T. M. Kamenecka, P. J. Kenny and J. Lindstrom (2015). "An Accessory Agonist Binding Site Promotes Activation of α4β2* Nicotinic Acetylcholine Receptors." J Biol Chem 290(22): 13907-13918.
Wang, J. and J. Lindstrom (2018). "Orthosteric and allosteric potentiation of heteromeric neuronal nicotinic acetylcholine receptors." Br J Pharmacol 175(11): 1805-1821.
Wevers, A., L. Monteggia, S. Nowacki, W. Bloch, U. Schütz, J. Lindstrom, E. F. Pereira, H. Eisenberg, E. Giacobini, R. A. de Vos, E. N. Steur, A. Maelicke, E. X. Albuquerque and H. Schröder (1999). "Expression of nicotinic acetylcholine receptor subunits in the cerebral cortex in Alzheimer's disease: histotopographical correlation with amyloid plaques and hyperphosphorylated-tau protein." Eur J Neurosci 11(7): 2551-2565.
Whiting, P. J., R. Schoepfer, W. G. Conroy, M. J. Gore, K. T. Keyser, S. Shimasaki, F. Esch and J. M. Lindstrom (1991). "Expression of nicotinic acetylcholine receptor subtypes in brain and retina." Brain Res Mol Brain Res 10(1): 61-70.
Wolfes, A. C. and C. Dean (2020). "The diversity of synaptotagmin isoforms." Curr Opin Neurobiol 63: 198-209.
Woolf, N. J. and L. L. Butcher (2011). "Cholinergic systems mediate action from movement to higher consciousness." Behav Brain Res 221(2): 488-498.
Xiao, C., J. M. Miwa, B. J. Henderson, Y. Wang, P. Deshpande, S. L. McKinney and H. A. Lester (2015). "Nicotinic receptor subtype-selective circuit patterns in the subthalamic nucleus." J Neurosci 35(9): 3734-3746.

Xiao, C., R. Nashmi, S. McKinney, H. Cai, J. M. McIntosh and H. A. Lester (2009). "Chronic nicotine selectively enhances alpha4beta2* nicotinic acetylcholine receptors in the nigrostriatal dopamine pathway." J Neurosci 29(40): 12428-12439.
Xu, J., T. Mashimo and T. C. Südhof (2007). "Synaptotagmin-1, -2, and -9: Ca(2+) sensors for fast release that specify distinct presynaptic properties in subsets of neurons." Neuron 54(4): 567-581.
Yang, Y., C. D. Paspalas, L. E. Jin, M. R. Picciotto, A. F. Arnsten and M. Wang (2013). "Nicotinic α7 receptors enhance NMDA cognitive circuits in dorsolateral prefrontal cortex." Proc Natl Acad Sci U S A 110(29): 12078-12083.
Young, J. W., N. Crawford, J. S. Kelly, L. E. Kerr, H. M. Marston, C. Spratt, K. Finlayson and J. Sharkey (2007). "Impaired attention is central to the cognitive deficits observed in alpha 7 deficient mice." Eur Neuropsychopharmacol 17(2): 145-155.
Zaborszky, L., A. Csordas, K. Mosca, J. Kim, M. R. Gielow, C. Vadasz and Z. Nadasdy (2015). "Neurons in the basal forebrain project to the cortex in a complex topographic organization that reflects corticocortical connectivity patterns: an experimental study based on retrograde tracing and 3D reconstruction." Cereb Cortex 25(1): 118-137.
Zenisek, D. (2008). "Vesicle association and exocytosis at ribbon and extraribbon sites in retinal bipolar cell presynaptic terminals." Proc Natl Acad Sci U S A 105(12): 4922-4927.
Zhou, F. M., Y. Liang and J. A. Dani (2001). "Endogenous nicotinic cholinergic activity regulates dopamine release in the striatum." Nat Neurosci 4(12): 1224-1229.
Zhou, Q. (2023). "Calcium Sensors of Neurotransmitter Release." Adv Neurobiol 33: 119-138.
Zoli, M., S. Pucci, A. Vilella and C. Gotti (2018). "Neuronal and Extraneuronal Nicotinic Acetylcholine Receptors." Curr Neuropharmacol 16(4): 338-349.
Zwart, R., L. M. Broad, Q. Xi, M. Lee, M. Moroni, I. Bermudez and E. Sher (2006). "5-I A-85380 and TC-2559 differentially activate heterologously expressed alpha4beta2 nicotinic receptors." Eur J Pharmacol 539(1-2): 10-17.

Appendix 1

Evaluation of the impact of pharmacological agents on the area under the curve of α4β2 responses versus cellular stability during patch-clamp recordings.

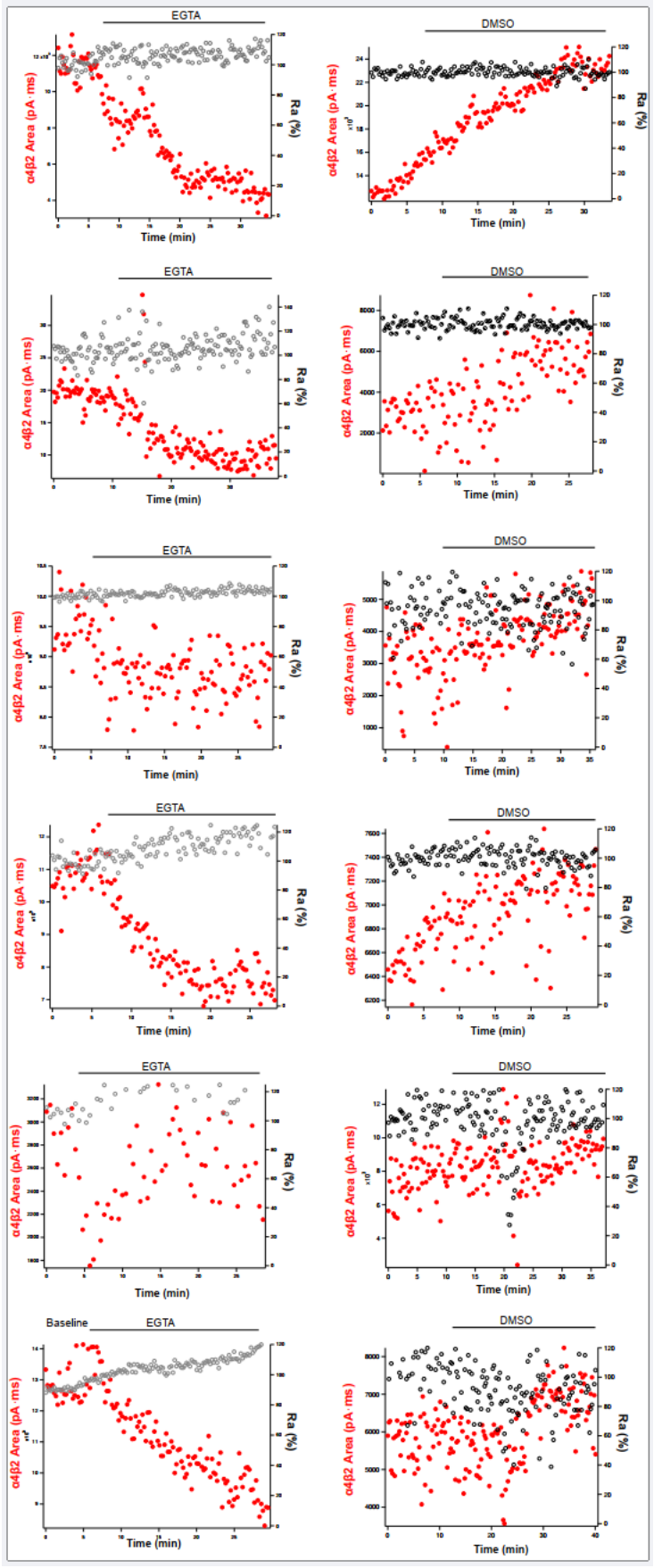

Effect of EGTA-AM on α7 Responses

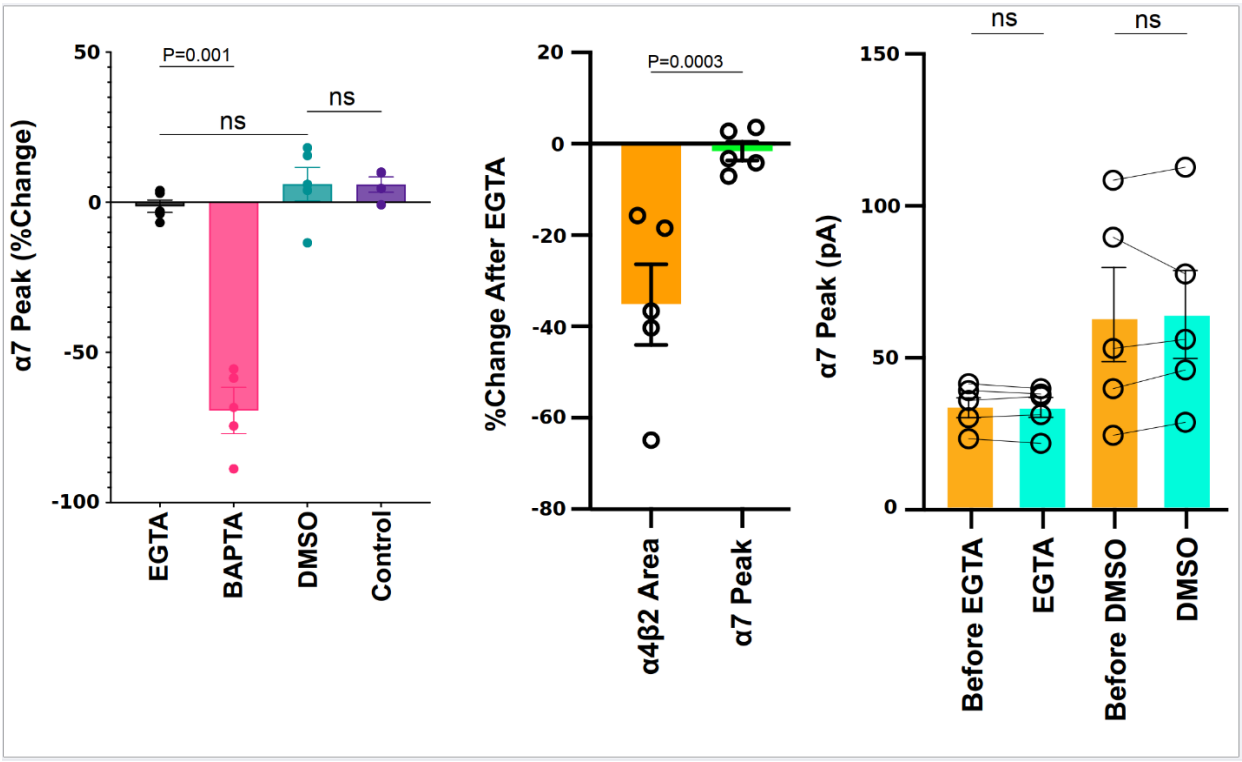

Statistical Analyses

MLA Peak of α7 (Figure 3-1C)

"Ratio paired t-test"
" P value" 0.0312
" P value summary" *
" Significantly different (P < 0.05)?" Yes
" One, or two-tailed P value?" One-tailed
" Sum of signed ranks (W)" -15.00
" Number of pairs" 5

DHβE Area of α4β2 Wilcoxon Matched-Pairs Signed Rank Test (Figure 3-1D)

P value: 0.0312
P value summary: *
Significantly different (P < 0.05)?: Yes
One- or two-tailed P value?: One-tailed
Number of pairs: 5

Time to peak (Figure 3-1F)

"Unpaired t-test"
" P value" <0.0001
" P value summary" ****
" Significantly different (P < 0.05)?" Yes
" One- or two-tailed P value?" One-tailed
" Welch-corrected t, df" "t=−20.83, df=10.00"

Peak to decay (Figure 3-1G)

"Ratio paired t-test"
" P value" <0.0001
" P value summary" ****
" Significantly different (P < 0.05)?" Yes
" One- or two-tailed P value?" One-tailed
" Welch-corrected t, df" "t=13.32, df=9.005"

Onset (Figure 3-1H)

"Ratio paired t-test"
" P value" 0.4912
" P value summary" ns
" Significantly different (P < 0.05)?" No
" One- or two-tailed P value?" One-tailed
" Welch-corrected t, df" "t=0.02239, df=17.76"

Peak of α7 EGTA (Figure 3-2C)
"Ratio paired t-test"
" P value" 0.7170
" P value summary" ns
" Significantly different (P < 0.05)?" No
" One- or two-tailed P value?" One-tailed
" t, df" "t=0.69, df=4"

Peak of α7 BAPTA (Figure 3-2C)
"Ratio paired t-test"
" P value" 0.01285
" P value summary" *
" Significantly different (P < 0.05)?" Yes
" One- or two-tailed P value?" One-tailed
" t, df" "t=4.131, df=4"

%Peak of α7 EGTA BAPTA (Figure 3-2D)
"Unpaired t-test with Welch's correction"
" P value" 0.0010
" P value summary" **
" Significantly different (P < 0.05)?" Yes
" One- or two-tailed P value?" One-tailed
" t, df" "t=8.531, df=3.432"

Area of α4β2 EGTA (Figure 3-2E)
"Ratio paired t-test"
" P value" 0.022
" P value summary" *
" Significantly different (P < 0.05)?" Yes
" One- or two-tailed P value?" One-tailed
" t, df" "t=2.0150, df=5"

Area of α4β2 BAPTA (Figure 3-2E)
"Ratio paired t-test"
" P value" 0.0002
" P value summary" *
" Significantly different (P < 0.05)?" Yes
" One- or two-tailed P value?" One-tailed
" t, df" "t=2.1318, df=4"

%Area of α4β2 EGTA BAPTA (Figure 3-2F)
"% decrease EGTA vs % decrease BAPTA"
"Unpaired t-test"
" P value" 0.00565
" P value summary" **
" Significantly different (P < 0.05)?" Yes

" One- or two-tailed P value?" One-tailed
" t, df" "t=−3.174, df=9"

Asynch EGTA (Figure 3-5E)
"Ratio paired t-test"
" P value" 0.0001
" P value summary" ***
" Significantly different (P < 0.05)?" Yes
" One- or two-tailed P value?" One-tailed
" t, df" "t=9.77, df=5"

Asynch BAPTA (Figure 3-5E)
"Ratio paired t-test"
" P value" 0.0019
" P value summary" **
" Significantly different (P < 0.05)?" Yes
" One- or two-tailed P value?" One-tailed
" t, df" "t=8.160, df=4"

Spontaneous Events EGTA (Figure 3-5F)
"Ratio paired t-test"
" P value" 0.001
" P value summary" **
" Significantly different (P < 0.05)?" Yes
" One- or two-tailed P value?" One-tailed
" t, df" "t=0.5680, df=5"

Spontaneous Events BAPTA (Figure 3-5F)
"Ratio paired t-test"
" P value" 0.0019
" P value summary" **
" Significantly different (P < 0.05)?" Yes
" One- or two-tailed P value?" One-tailed
" t, df" "t=8.160, df=4"

%SQRT BAPTA EGTA (Figure 3-6B)
"Unpaired t-test with Welch's correction"
" P value" 0.0054
" P value summary" **
" Significantly different (P < 0.05)?" Yes
" One- or two-tailed P value?" One-tailed
" t, df" "t=4.020, df=4.848"

SQRT EGTA (Figure 3-6B)
"Ratio paired t-test"
" P value" 0.023
" P value summary" *
" Significantly different (P < 0.05)?" Yes

" One- or two-tailed P value?" One-tailed
" t, df" "t=2.614, df=5"

SQRT BAPTA (Figure 3-6B)
"Ratio paired t-test"
" P value" 0.0035
" P value summary" *
" Significantly different (P < 0.05)?" Yes
" One- or two-tailed P value?" One-tailed
" t, df" "t=5.09, df=4"

%SQRT DMSO (Figure 3-6C)
"Ratio paired t-test"
" P value" 0.0011
" P value summary" *
" Significantly different (P < 0.05)?" Yes
" One- or two-tailed P value?" Two-tailed
" t, df" "t=−3.623, df=4"

%SQRT aCSF (Figure 3-6C)
"Ratio paired t-test"
" P value" 0.0016
" P value summary" **
" Significantly different (P < 0.05)?" Yes
" One- or two-tailed P value?" Two-tailed
" t, df" "t=−11.086, df=3"

MLA Asynchronous events (Figure 3-7E)
"Ratio paired t-test"
" P value" 0.125
" P value summary" ns
" Significantly different (P < 0.05)?" No
" One- or two-tailed P value?" One-tailed
" Sum of signed ranks (W)" 13.00
" Number of pairs" 5

Asynchronous events DHβE (Figure 3-7E)
"Ratio paired t-test"
" P value" 0.0017
" P value summary" **
" Significantly different (P < 0.05)?" Yes
" One- or two-tailed P value?" One-tailed
" t, df" "t=7.439, df=4"

MLA Spontaneous Events (Figure 3-7F)
"Ratio paired t-test"
" P value" 0.21875
" P value summary" ns

" Significantly different (P < 0.05)?" No
" One- or two-tailed P value?" One-tailed
" Sum of signed ranks (W)" 7.000
" Number of pairs" 5

%Peak of α7 DMSO (Figure 3-8C)
"Unpaired t-test with Welch's correction"
" P value" 0.49105
" P value summary" ns
" Significantly different (P < 0.05)?" No
" One- or two-tailed P value?" One-tailed
" t, df" "t=0.02344, df=5.546"

%Peak of α7 DMSO CONTROL (Figure 3-8C)
"Unpaired t-test with Welch's correction"
" P value" 0.49105
" P value summary" ns
" Significantly different (P < 0.05)?" No
" One- or two-tailed P value?" One-tailed
" t, df" "t=0.02344, df=5.546"

Area of α4β2 DMSO (Figure 3-8D)
"Ratio paired t-test"
" P value" 0.0002
" P value summary" ***
" Significantly different (P < 0.05)?" Yes
" One- or two-tailed P value?" One-tailed
" t, df" "t=−10.751, df=4"

Area of α4β2 aCSF (Figure 3-8D)
"Ratio paired t-test"
" P value" 0.008
" P value summary" *
" Significantly different (P < 0.05)?" Yes
" One- or two-tailed P value?" One-tailed
" t, df" "t=4.303, df=3"

%Area of α4β2 Non DMSO Control vs DMSO (Figure 3-8D)
"Unpaired t-test with Welch's correction"
" P value" 0.07645
" P value summary" ns
" Significantly different (P < 0.05)?" No
" One- or two-tailed P value?" One-tailed
" t, df" "t=1.857, df=3.258"

DMSO Asynchronous events (Figure 3-8G)
"Ratio paired t-test"
" P value" 0.0548
" P value summary" ns

" Significantly different (P < 0.05)?" No
" One- or two-tailed P value?" One-tailed
" t, df" "t=−2.051, df=4"

aCSF CONTROL Asynchronous events (Figure 3-8G)
"Ratio paired t-test"
" P value" 0.05385
" P value summary" ns
" Significantly different (P < 0.05)?" No
" One- or two-tailed P value?" One-tailed
" t, df" "t=2.272, df=3"

DHβE Asynchronous events (Figure 3-8G)
"Ratio paired t-test"
" P value" 0.0017
" P value summary" **
" Significantly different (P < 0.05)?" Yes
" One- or two-tailed P value?" One-tailed
" t, df" "t=7.439, df=4"
" Number of pairs" 5

Spontaneous Events DMSO (Figure 3-8H)
"Ratio paired t-test"
" P value" 0.156
" P value summary" ns
" Significantly different (P < 0.05)?" No
" One- or two-tailed P value?" One-tailed
" t, df" "t=4.041, df=4"

Spontaneous Events aCSF (Figure 3-8H)
"Ratio paired t-test"
" P value" 0.03875
" P value summary" *
" Significantly different (P < 0.05)?" Yes
" One- or two-tailed P value?" One-tailed
" t, df" "t=2.642, df=3"

Nifedipine Spontaneous Events (Figure 3-9C)
"Wilcoxon matched-pairs signed rank test"
" P value" 0.0312
" P value summary" *
" Significantly different (P < 0.05)?" Yes
" One- or two-tailed P value?" One-tailed
" Number of pairs" 5

Nifedipine Asynchronous events (Figure 3-9D)
"Paired t-test"
" P value" 0.0389
" P value summary" *
" Significantly different (P < 0.05)?" Yes

" One- or two-tailed P value?" One-tailed
" t, df" "t=2.358, df=4"
" Number of pairs" 5

Area of α4β2 (Figure 3-9E)
"Ratio paired t-test"
" P value" 0.0002
" P value summary" ***
" Significantly different (P < 0.05)?" Yes
" One- or two-tailed P value?" One-tailed
" t, df" "t=−10.751, df=4"

Nifedipine Peak (Figure 3-9F)
"Ratio paired t-test"
" P value" 0.0720
" P value summary" ns
" Significantly different (P < 0.05)?" No
" One- or two-tailed P value?" One-tailed
" t, df" "t=1.814, df=4"
" Number of pairs" 5

Atropine Area of α4β2 (Set 1) (Figure 3-10C)
"Ratio paired t-test"
" P value" 0.00715
" P value summary" **
" Significantly different (P < 0.05)?" Yes
" One- or two-tailed P value?" One-tailed
" t, df" "t=4.144, df=4"

Atropine Peak of α7 (Figure 3-10D)
"Ratio paired t-test"
" P value" 0.4292
" P value summary" ns
" Significantly different (P < 0.05)?" No
" One- or two-tailed P value?" One-tailed
" t, df" "t=0.1902, df=4"

Atropine Spontaneous Events (Set 3) (Figure 3-10E)
"Ratio paired t-test"
" P value" 0.15005
" P value summary" ns
" Significantly different (P < 0.05)?" No
" One- or two-tailed P value?" One-tailed
" t, df" "t=1.189, df=4"

Atropine Asynchronous events (Set 2) (Figure 3-10F)
"Ratio paired t-test"
" P value" 0.0653
" P value summary" ns
" Significantly different (P < 0.05)?" No

" One- or two-tailed P value?" One-tailed
" t, df" "t=1.897, df=4"

Ca Asynchronous events 1 vs 2 (Figure 3-11E)
"Ratio paired t-test"
" P value" <0.0001
" P value summary" ****
" Significantly different (P < 0.05)?" Yes
" One- or two-tailed P value?" One-tailed
" Mann-Whitney U" 19

Ca Asynchronous events 2 vs 3 (Figure 3-11E)
"Ratio paired t-test"
" P value" 0.00565
" P value summary" **
" Significantly different (P < 0.05)?" Yes
" One- or two-tailed P value?" One-tailed
" Welch-corrected t, df" "t=2.654, df=40.26"

Ca Asynchronous events 3 vs 5 (Figure 3-11E)
"Ratio paired t-test"
" P value" 0.1961
" P value summary" ns
" Significantly different (P < 0.05)?" No
" One- or two-tailed P value?" One-tailed
" Mann-Whitney U" 246

Ca Spontaneous Events 1 vs 2 (Figure 3-11F)
"Ratio paired t-test"
" P value" 0.09965
" P value summary" ns
" Significantly different (P < 0.05)?" No
" One- or two-tailed P value?" One-tailed
" Mann-Whitney U" 231

Ca Spontaneous Events 3 vs 5 (Figure 3-11F)
"Ratio paired t-test"
" P value" 0.3837
" P value summary" ns
" Significantly different (P < 0.05)?" No
" One- or two-tailed P value?" One-tailed
" Welch-corrected t, df" "t=0.2977, df=40.83"

Spontaneous Events Ca2 vs 3 (Figure 3-11F)
"Ratio paired t-test"
" P value" 0.01995
" P value summary" *
" Significantly different (P < 0.05)?" Yes
" One- or two-tailed P value?" One-tailed
" Mann-Whitney U" 197